Quantifying the slip rates, spatial distribution and evolution of active normal faults from geomorphic analysis: Field examples from an oblique-extensional graben, southern Turkey

Sarah J. Boulton [a, *] & Alexander C. Whittaker[b]

[a]School of Earth, Ocean and Environmental Science, University of Plymouth, Drake Circus, Plymouth, Devon, PL4 8HS, UK

[b]Department of Earth Science and Engineering, Royal School of Mines, Imperial College, London, SW7 2AZ, UK

[*] Corresponding author. Tel: + 44175 584762; Fax: +441752 233117; E-mail: sarah.boulton@plymouth.ac.uk

Abstract

Quantifying the extent to which geomorphic features can be used to extract tectonic signals is a key challenge in the Earth Sciences. Here we analyse the drainage patterns, geomorphic impact, and long profiles of bedrock rivers that drain across and around normal faults in a regionally significant oblique-extensional graben in southern Turkey that has been mapped geologically, but for which there are poor constraints on the activity, slip rates and Plio-Pleistocene evolution of basin-bounding faults. We show that drainage in the graben is strongly asymmetric, and by mapping the distribution of wind gaps, we are able to evaluate how the drainage network has evolved through time. By comparing the presence, size, and distribution of long profile convexities, we demonstrate that the northern margin of the graben is tectonically quiescent, whereas the southern margin is bounded by active faults. Our analysis suggests that rivers crossing these latter faults are undergoing a transient response to ongoing tectonic uplift, and this interpretation is supported by classic signals of transience such as gorge formation and hill slope rejuvenation within the convex reach. Additionally, we show that the height of long profile convexities varies systematically along the strike of the southern margin faults, and we argue that this effect is best explained if fault linkage has led to an increase in slip rate on the faults through time from ~ 0.1 to 0.45 mm/yr. By measuring the average length of the original fault segments, we estimate the slip rate enhancement along the faults, and thus calculate the range of times for which fault acceleration could have occurred, given geological estimates of fault throw. These values are compared with the times and slip rates required to grow the documented long-profile convexities enabling us to quantify both the present-day slip rate on the fault (0.45 ± 0.05 mm/yr) and the timing of fault acceleration (1.4 ± 0.2 Ma). Our results have substantial implications for predicting earthquake hazard in this densely populated area (calculated potential M_w = 6.0-6.6), enable us to constrain the tectonic evolution of the graben through time, and more widely, demonstrate that geomorphic analysis can be used as an effective tool for estimating fault slip rates over time periods > 10^6 years, even in the absence of direct geodetic constraints.

Keywords: neotectonics; eastern Mediterranean; fault evolution; drainage patterns; long profile; seismic hazard; tectonic geomorphology

1. Introduction

In recent years, interest has increased in using geomorphologic features to investigate the neotectonics of actively deforming regions (Merritts and Vincent, 1989; Leeder and Jackson, 1993; Goldsworthy and Jackson, 2000; Kirby and Whipple, 2001; Lavé and Avouac, 2001; Wobus et al., 2006). This focus is largely attributable to the realisation that as tectonics exerts a first-order control on landscape through the production or modification of geomorphic features, then in principle it should be possible to deduce the nature and potentially the magnitude of tectonic forcing from field observation and measurement of key geomorphic features (Burbank and Anderson, 2001). Such an approach would be particularly useful where direct geological, structural or geodetic constraints are unavailable (e.g., Kirby and Whipple, 2001; Whittaker et al., 2008).

The fluvial system in particular has become the focus for much work in this field. This is because rivers are the primary agents by which tectonic signals are transmitted to the surrounding landscape (e.g., Tucker and Bras, 1998; Snyder et al., 2000) and hence are responsible for setting hill-slope gradients and topographic relief (Whipple and Tucker, 1999; Whipple, 2004). In addition, they export geologically significant quantities of sediment from upland regions to neighbouring basins or to the oceans each year (Milliman and Syvitski, 1992). Moreover, because the component parts of the fluvial system can respond over differing time periods (from individual channels to the drainage network as a whole), they offer the opportunity to examine response timescales in tectonically forced landscapes (Snyder et al., 2000; Whittaker et al., 2007b). Studies considering drainage pattern evolution in both fold and thrust belts (Burbank et al., 1986; Jackson et al., 1996; Keller et al., 1999) and in extensional grabens (Paton, 1992; Leeder and Jackson, 1993;

Goldsworthy and Jackson, 2000; Zelilidis, 2000) also demonstrate how drainage patterns can be used to document the evolution of fault propagation over time periods > 1 My. Recent modelling work by Cowie et al. (2006) explicitly shows how drainage networks are sensitive to the growth and interaction of faults and, hence how their network properties can be used to interpret the temporal and spatial history of active faulting in extensional settings, such as the central Apennines of Italy and the Gulf of Evia, Greece.

The longitudinal profiles of rivers in areas of active tectonics have also been the focus of substantial research activity (Merritts and Vincent, 1989; Snyder et al., 2000; Kirby et al., 2003; Whittaker et al., 2007a). Tectonically unperturbed "equilibrium" fluvial long profiles are typically smooth and concave-up, representing a balance between downstream reduction in gradient and concomitant increase in discharge. However, upland rivers are also sensitive to along-stream variations in differential uplift (potentially leading to changes in the profile concavity or steepness index) and also to changes in uplift rate through time (Kirby et al., 2003; Wobus et al., 2006). In particular, modelling work by Whipple and Tucker (2002) demonstrated that a diagnostic response for any river incising bedrock that is limited by its capacity to detach material from its bed, and responding to an increase in relative uplift rate (whether caused by tectonics or base-level fall), is the development of a transient "knickzone" or convex reach that propagates upstream as the channel successively adjusts to the imposed uplift field. Recent field evidence from the central Apennines confirms the existence of such transient river responses to tectonics and suggests that the response timescale of upland fluvial systems with drainage areas < 100 km^2 to such perturbations is > 1 My (Whittaker et al., 2007a, b). Moreover, modelling work, theory, and new field observations suggest that the vertical elevation of long-profile convexities scales with fault slip rate (Niemann et al., 2001; Whittaker et al., 2008; Attal et al., 2008). This raises the prospect of being able to decode transient fluvial landscapes to gain quantitative information about regional tectonics over timescales > 10^6 years.

Unfortunately, few current studies effectively combine these methodologies together. Existing work on drainage network evolution is often limited to geomorphically qualitative inferences (Leeder and Jackson, 1993; Jackson et al., 1996) or is content to demonstrate that documented geomorphic features are broadly consistent with a tectonic and geodetic framework derived from other means (e.g., Goldsworthy and Jackson, 2000). Moreover, these studies do not integrate detailed studies of river long profiles. On the other hand, a plethora of research has evaluated fluvial profiles in tectonically active areas, but many of these studies have either explicitly or implicitly assumed that the landscape is in topographic steady-state (e.g., Kirby et al., 2003; Wobus et al., 2006), are largely concerned with calibrating fluvial incision laws (e.g., Van der Beek and Bishop, 2003), or are focussed on evaluating the applicability of hydraulic scaling relationships to tectonically perturbed channels (Duvall et al., 2004; Finnegan et al., 2005; Whittaker et al., 2007a). This means that few workers have succeeded in extracting detailed and/or novel inferences about regional tectonic forcing from integrated analyses of long profile and drainage network data in areas where the neotectonic framework is presently poorly constrained.

This paper seeks to address this outstanding challenge. We combine a range of geomorphologic techniques with available structural and geological data to decipher the neotectonics of a regionally significant Plio-Quaternary Graben in southern Turkey (the Hatay Graben), where the rates and timing of fault motion are presently poorly constrained. In particular, we analyse the drainage patterns in the area to clarify the development of the large-scale basin-bounding faults, and we compare the location and distribution of wind gaps with the position of known faults. Additionally, we examine the long profiles of channels crossing the present basin margins; and by quantifying the presence, size, and distribution of long profile convexities we deduce which structures are likely to be active at the present time. Significantly, our data and observations also allow us to estimate the rates and timing of fault motion in the area and to reconstruct the tectonic evolution of the graben through time. The results are important in terms of geological development of the eastern Mediterranean region and also for hazard prediction in the

local area. More widely, this study demonstrates that geomorphological analysis is now a powerful tool to evaluate tectonics, even in the absence of direct geodetic observations.

2. Geological setting

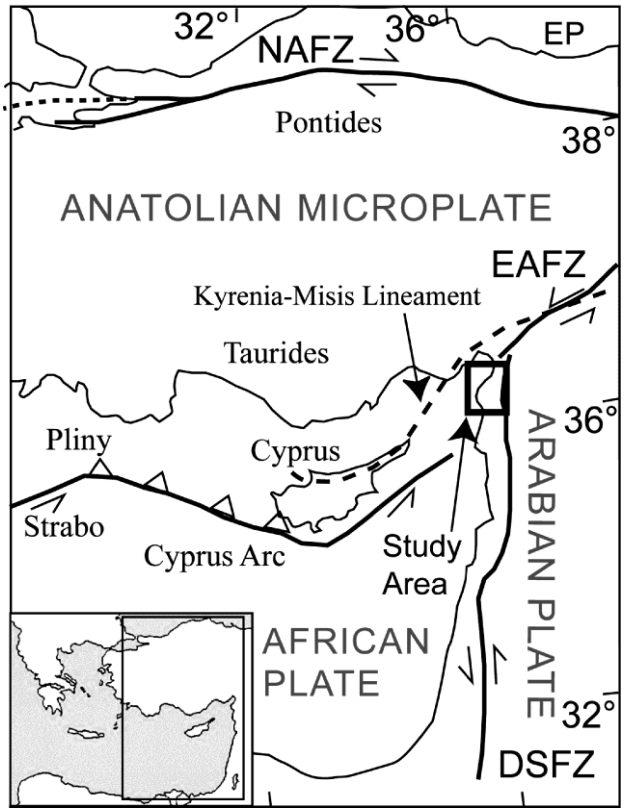

Figure 1 Plate tectonic map of the eastern Mediterranean, showing the major neotectonic lineaments (NAFZ – North Anatolian Fault Zone; EAFZ – East Anatolian Fault Zone; DSFZ – Dead Sea Fault Zone) and the location of the study area (box).

The eastern Mediterranean region is dominated by large strike-slip faults that have developed during the Pliocene as a result of the northward motion of Africa into Eurasia. During the Pliocene, the Anatolian microplate formed (Fig. 1), with the North Anatolian Fault Zone (NAFZ) and the East Anatolian Fault Zone (EAFZ) as the northern and southeastern plate boundaries, respectively (Fig. 1). The NAFZ is a dextral strike-slip fault that formed in the earliest Pliocene (~ 5 Ma; Barka and Kadinsky-Cade, 1988); whereas, the EAFZ is a sinistral strike-slip fault, the timing of which is not so well constrained as the NAFZ, with the age given as Late Miocene-Early Pliocene (Şengör et al., 1985; Arpat and Şaroğlu, 1972) or Late Pliocene (Yürür and Chorowicz, 1998; Westaway and

Arger, 1998). Additionally during the Miocene, rifting initiated in the Red Sea and the differential motion between Africa and Arabia resulted in the formation of the sinistral Dead Sea Fault Zone (DSFZ). The first motion along the DSFZ occurred in the south sometime in the Miocene, variously dated as < 20 Ma (Lyberis, 1988), 18 Ma (Garfunkel and Ben Avraham, 1996), Late Miocene (Steckler et al., 1988) and has subsequently propagated northward throughout the Pliocene.

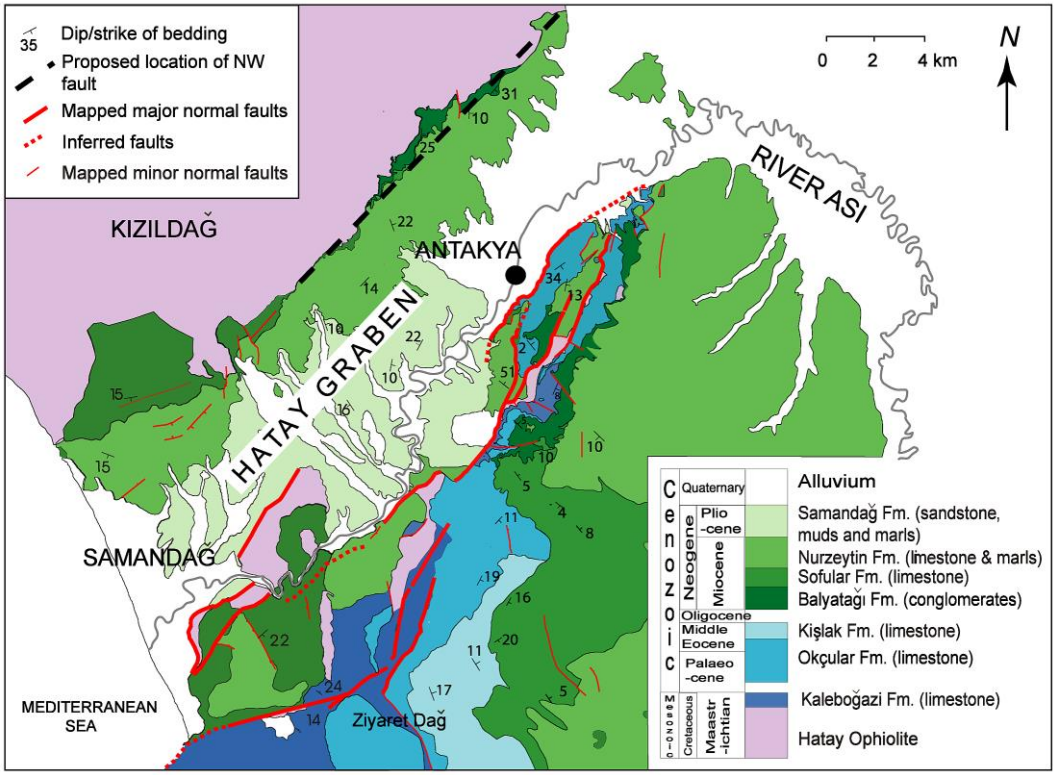

Figure 2. Simplified geological map of the Hatay region of Southern Turkey. Note the predominance of faulting in the SE forming the southern boundary of the Hatay Graben. By contrast only shorter, smaller faults without significant displacement are present along the northern boundary, which is delineated by the change in lithology from sedimentary to ophiolitic rocks. Although a large fault has been proposed to run along this lithological contact, no evidence for it was observed during field work.

The Hatay Graben is a Plio-Quaternary basin (Boulton et al., 2006; Boulton and Robertson, 2008) located in south-central Turkey (Fig. 1) adjacent to the northern part of the DSFZ. The graben is orientated NE-SW and is ~ 20 km wide and over 50 km in length. To the NW it is bounded by the Kızıldağ (Fig. 2), a range of mountains that extend northward for about 80 km and rise sharply from the Mediterranean Sea and the Gulf of Iskenderun to ~ 1800 m in height. To the SE, the basin is bounded by the mountains of Zıyaret Dağ, which rise to ~ 1300 m. The Hatay Graben is a

topographic low formed because of oblique-extension along the dominantly NE-SW trending normal faults that strike parallel to these mountain fronts (Boulton et al., 2006). The flanks of the graben are dominated by basement serpentinite and Middle Miocene bioclastic limestones, while Upper Miocene marls and Pliocene to Recent sandstones and conglomerates outcrop in the axial zone (Fig. 2) (Boulton et al., 2006, 2007; Boulton and Robertson, 2007). The asymmetric topography of the graben (inset, Fig. 3) is apparently controlled by large en-echelon normal faults on the SE margin with minor antithetic normal and strike-slip faults in the NW (Boulton and Robertson, 2008); however, a large SE-dipping normal fault has also been postulated to be present along the entire northern margin of the basin (Yürür and Chorowicz, 1998). At least two sets of faults bound the southern margin of the basin (Fig 2); the innermost array currently runs close to the margin of the basin, with further faults exposed at higher elevations within the Zıyaret Dağ. Detailed structural mapping (Boulton, 2006) shows that these faults are typically segmented over the length-scale of ~ 5 km (Fig. 2), with estimated Early Pliocene to Recent maximum throw on the inner-bounding fault of ~ 1000 m east of the city of Antakya; total throw on this fault since the base of the Upper Miocene is 1500 m, based upon stratigraphic piercing points. Additionally, at least 500 m of throw has been calculated for the fault segment bounding the Samandağ mountain. Throw on the outer fault set is less well constrained but is estimated to be < 500 m (Boulton et al., 2006).

The area (from 35.9º N to 36.75º N, 35.76º E to 36.7º E) has experienced at least 32 earthquakes in the last 20 years [body wave magnitude ≤ 5.7] (USGS National Earthquake Information Centre) showing that the Hatay Graben is still undergoing active extension. Focal plane mechanisms of recent shallow earthquakes suggest the faults to be dip-slip to oblique-slip in nature (Erdik et al., 1997; Över et al., 2002; Harvard CMT catalogue). Although there are some uncertainties in the epicentral location, the error is of the order of 10-20 km (Jackson, 2001), which places these earthquakes firmly within the graben. In addition, Global Positioning System (GPS) measurements can provide information on current plate motions. Geodetic data from McClusky et al. (2000) showed that in an Arabian fixed reference frame GPS vectors are oppositely oriented across the

Hatay Graben, indicating the area is experiencing oblique-extension. However, lack of fresh scree, unweathered fault scarps, and surface ruptures mean that active faults have not been unambiguously identified in the field.

Although timing of initial normal fault motion has been established stratigraphically as commencing during the Middle Miocene (Boulton et al., 2006), this faulting apparently resulted from far-field stresses related to continental collision to the north and did not immediately lead to graben formation (Boulton and Robertson, 2007), with Middle Miocene syn-rift sedimentation being entirely marine (Boulton et al., 2006). Instead, it is thought that these early normal faults were reactivated during the Pliocene resulting in the development of the present subaerial graben as global sea level fell from 5 Ma onward and as regional uplift took place (Boulton et al., 2006; Boulton and Robertson, 2008). This resulted in the deposition of > 100 m of Plio-Pleistocene coastal and fluvial sediments which are completely confined to the basin, the lowermost of which are shallow marine and dated by micropalaeontological and strontium isotopic analysis to be no younger than 5.2 My (Boulton et al., 2007). A significant drainage network was therefore established on the graben flanks by 5 Ma. The chronology of fault motion is based upon a number of observations, such as fanning Middle and Upper Miocene sediments, differential elevations of intially contiguous Messinian evaporites, highly deformed Pliocene sediments adjacent to fault planes, and variation in dips of Quaternary talus (for a full discussion see Boulton et al., 2006). However, key questions remain unanswered. In particular, the spatial and temporal development of the graben through the Pliocene to Recent is largely unknown, as are the current rates and distributions of active faults (see above). These questions are significant for understanding the tectonic development of this key area in the eastern Mediterranean. In particular, the graben's location at the interface between a collisional and precollisional tectonic setting, and in a zone of transtension resulting from the motion of Anatolia away from Arabia-Africa, means that a greater understanding of the regional fault dynamics could provide important constraints on existing models of plate motion for the eastern Mediterranean. In addition, a full knowledge of the location,

and enhanced constraints on the rates of active faults in the area would also signifiantly improve earthquake hazard assessment, a priority given the high population density in the region, particularly in and around the city of Antakya (ancient Antioch) located in the NE of the graben (Fig. 2).

3. Methodology and approach

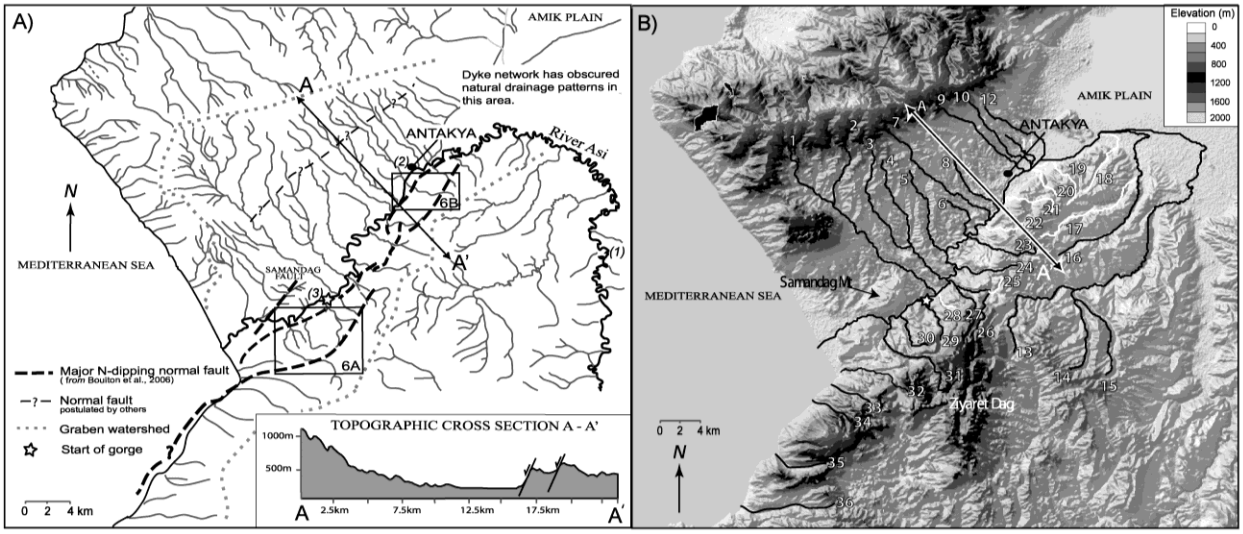

Figure 3. (A) Stream network map of the Hatay area. Inset shows topographic profile across the line A-A' and the boxes show location of maps in Fig. 6. Numbers 1-3 refer to the points on the River Asi profile shown in Fig. 5. (B) Colour-shaded DEM of the Hatay area, showing rivers 1-36, which were extracted for long profile analysis and are presented in Figs. 7-9. Note that the channels in A were derived from "blue-lined" rivers on topographic maps, whereas in B the stream network was generated from the DEM used, thus there are some differences between the two networks shown.

We used the geological data described above in conjunction with an SRTM-derived digital elevation model (DEM) of the Hatay Graben and field reconnaissance of key study sites to document and quantify the geomorphic signature of the area's tectonic evolution. We analysed both regional drainage patterns in the Hatay province (section 4.1) and also conducted a quantitative study of river long profiles draining both flanks of the graben (section 4.2). To do this, a stream network with a threshold drainage area of 0.1 km^2 was derived from the DEM (Fig. 3A) and was verified against "blue-lined" rivers shown on (1:200 000) topographic survey maps and by field

inspection of selected channel sites. We also extracted long profiles and drainage areas, *A*, of 36 individual channels in the area (Fig. 3B). These streams

(i) drain the north side of the basin (rivers 1-12);

(ii) are sourced in the southeastern mountains (Zıyaret Dağı) and feed the Amik Plain (rivers 13-18);

(iii) incise across the normal fault-bounded SE margin of the Hatay Graben (rivers 19-31), and

(iv) drain directly into the Mediterranean Sea, SW of the Hatay Graben (rivers 31-36)

and therefore cover a wide range of tectonic and lithologic conditions shown in Fig. 2.

We also calculated, where appropriate, channel concavity, θ, and steepness index, k_s, for the streams (c.f., Kirby et al., 2003) from

$$S = k_s A^{-\theta} \quad (1)$$

where S is the local channel gradient. For comparative purposes as k_s depends on the concavity of the channel, we also quote the normalised steepness index, $k_{sn,}$ which for our purposes is equivalent to k_s using a reference concavity of 0.5. For channels that are in topographic steady-state and where there are no lithological variations, normalised steepness can be related to rates of rock uplift (see Wobus et al., 2006, for a detailed review).

Additionally, for each channel, we documented the presence of any prominent convexities in the long profile and recorded their position and size relative to the location of active faults in the area (c.f., Whittaker et al., 2008; Attal et al., 2008). Such profile convexities are developed as rivers near the detachment limited end-member respond to a change in uplift rate (see section 1). However, because channel long profiles often have small perturbations or knickpoints which can be related, amongst others, to small changes in rock strength or landslide dams, and hence do not just reflect tectonics, we concentrate in this paper on significant profile convexities (oversteepened reaches) that have vertical elevations of ~100 m or more, as measured from the mapped faults to the break in slope in the long profile (see also Fig. 10 in Whittaker et al., 2008). The break in slope is

identified as the point at which the rate of change of slope in the long profile reaches a local maximum upstream of the fault. Some channels do have more than one slope-break within a small upstream distance (i.e., 1-2 km). In such cases, we give a range of values for the profile convexity height.

Figure 4. (A) View of the lower reaches of the River Asi incising deeply through Middle Miocene limestones prior to flowing into the sea. (B) View of river one half to ~ 1 km before flowing out into the Hatay Graben; at this point the bedrock river is incising through the ophiolite–Middle Miocene boundary. (C) View downstream (toward the graben) of stream 20 as it incises through serpentinite exhumed in the footwall of the outer graben-bounding fault (the upper reaches of this stream can be seen in Fig. 12A). (D) View of the headwaters of stream 13 that drains eastward off the back of the Hatay Graben, showing the bedrock nature of the stream bed (the white line in the stream bed is an irrigation pipe).

Alongside the above, we also observed selected stream beds (Fig. 4) to document the typical fluvial incision process and to estimate the extent to which the channel incised bedrock. Finally, we noted any evidence for wind-gap formation (i.e., saddle points in valleys where drainage reversal had potentially occurred) and verified these sites in the field by inspection of sediments preserved within the potential wind gap (section 4.3). Note that small channels observed flowing off

Samandağ Mountain and elsewhere have been excluded from this study, because of their short lengths and drainage areas (< 4 km and 5 km^2, respectively) and evidence for debris-flow-dominated processes taking place within the channel.

4. Results

4.1. Overview of drainage in the Hatay Graben

Drainage in the Hatay basin is strongly asymmetric (Fig. 3). The axis of the Hatay Graben is drained by the River Asi (also known as the Orontes), a major water course draining northward from Syria to Turkey along the DSFZ. It is ~ 400 km long (drainage area > 30 000 km^2) and largely meandering in character, with bankfull channel widths exceeding 100 m at maximum extent. The River Asi enters the Hatay Graben NE of the city of Antakya, at the northern termination of the SE graben-bounding mountain front (Figs. 2, 3). Here, the river makes a sharp turn to the SW and then flows along the southeast side of the graben, close to the inner-most faults that bound this side of the graben. The river flows along the wide graben floor for > 30 km until it enters a gorge that has been incised into Samandağ Mountain (star, Fig. 3; photo, Fig. 4A), a feature that is mapped as fault-bounded to the north (Figs. 2, 3B). The gorge is cut into serpentinite and Middle Miocene limestones, is up to 200 m deep and at its narrowest, is < 100 m wide, compared with valley widths > 1 km upstream in the graben. The gorge ends near the village of Sutası, where the river flows over the boundary fault. The long profile of the River Asi (Fig. 5) shows the river to have a very low gradient: < 0.1° in the NE as it crosses the Amik plain, much of which was a shallow lake until the 1940s (Kilic et al., 2006). Elevation is not lost immediately as the river enters Hatay Graben; instead, the river starts to incise downstream of Antakya, ~ 35 km upstream of the sea (point 2, Figs. 3A; 5). The long profile steepens further as the river enters the gorge, losing an additional 40 m of elevation in just 10 km downstream (point 3, Figs. 3A; 5).

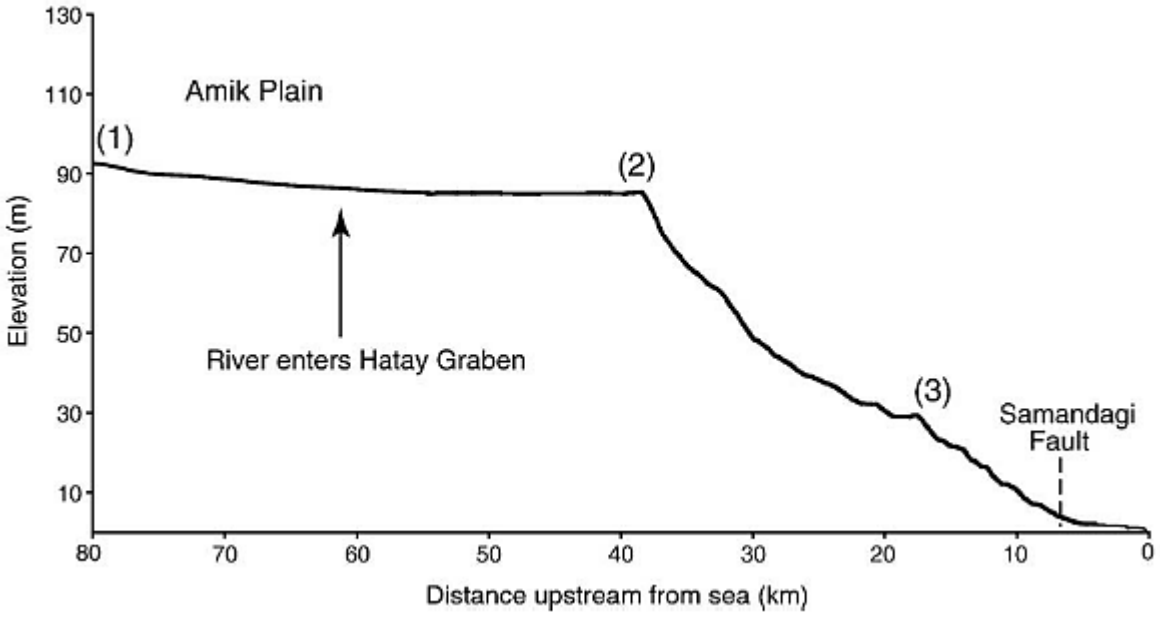

Figure 5 Long profile of the River Asi. Distances are measured upstream of the sea, and numbers correspond to localities in Fig. 3A.

The River Asi sets the base-level for all other channels draining the area. Tributaries draining into the axial river have been observed to be bedrock channels with variable (but minor) amounts of sediment load, with evidence for seasonal flow if they were observed to be dry during the field visit (Fig. 4). The larger channels, such as rivers 1-4, transport significant amounts of bedload in their lower reaches, but are bedrock channels in the upper sections. For example, although rivers 1-2 transport coarse bedload in the lower reaches and flows all year round, for more than half of the reach of the river (i.e., upstream of 15 km) it is a bedrock channel with > 50% exposed bedrock in the channel bottom. In places, the channel has incised > 150 m into the bedrock (Fig. 4B), and this is typical of the majority of the channels draining the NW margin of the graben. By contrast, most of the streams draining the SE graben margin are smaller streams with little bedload (Fig. 4C). Seasonal river flow has been witnessed in these streams in spring months and following heavy rain; in addition, bedrock in channel bottoms is polished and streams are clear of dense vegetation up to the headwaters. Sediments, where present, are well-sorted and imbricated, suggesting that fluvial rather than debris flow processes are responsible for cutting the channels. The lower reaches of these streams are well-incised (Fig. 4C), whereas the upper reaches sit in wide

valleys. Streams flowing east, away from the graben (rivers 13-18) also generally have wide open valleys with bedrock streams with little or no bedload (river 13; Fig. 4D); however, in these channels the degree of incision does not increase downstream.

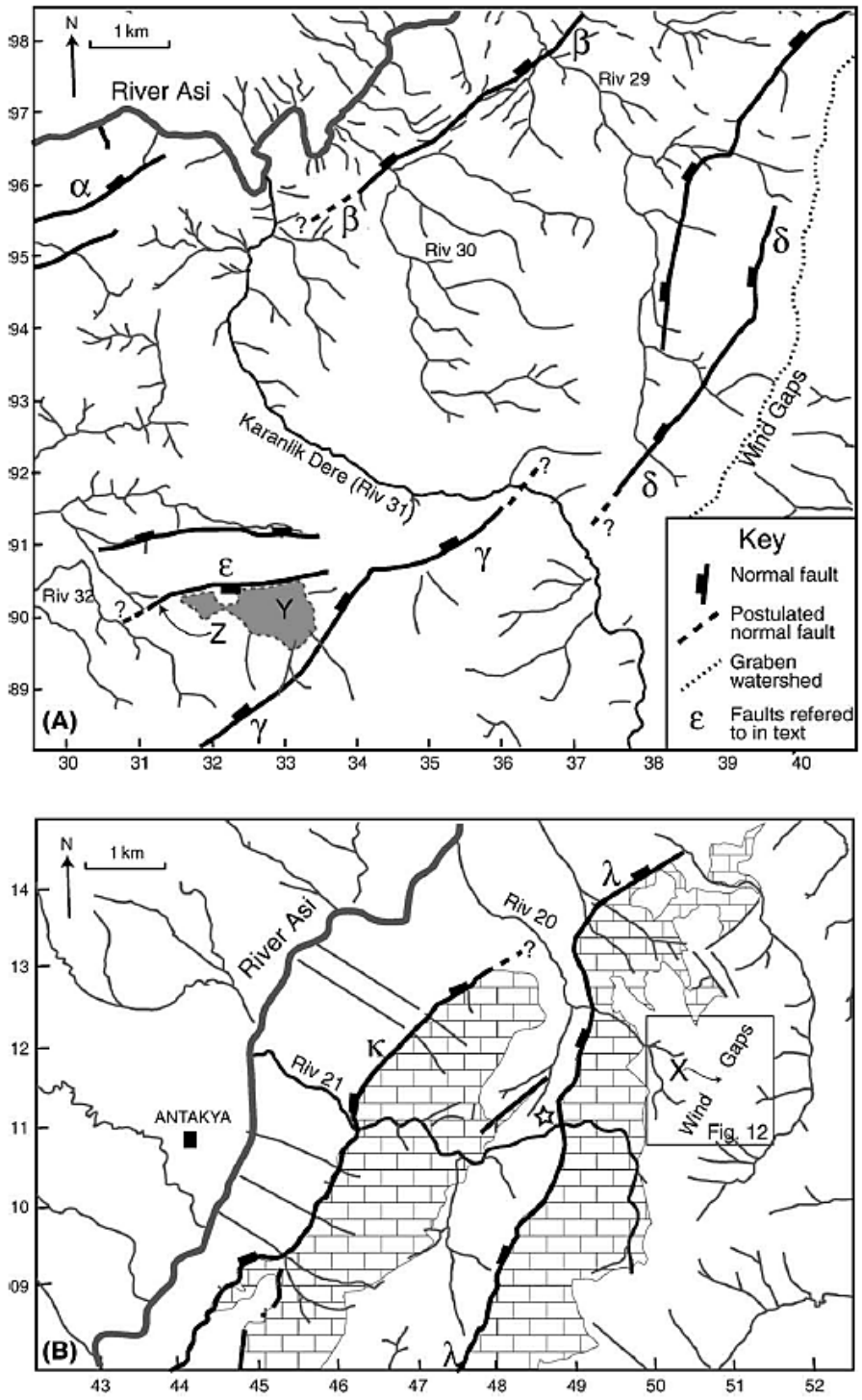

Figure 6. Detailed locality maps showing drainage patterns of rivers around mapped fault segments. Geographic localities of these maps are shown in Fig. 3A. Letters X, Y, and Z refer to localities mentioned explicitly in section 4.3. The grey shading in (A) represents the extent of the internally drained basin, Y; and the brick ornament in (B) represents carbonate bedrock.

In general, streams on the northwestern side of the graben are long with a well-developed network of tributaries (Fig. 3A). The rivers are well-incised forming steep, narrow valleys within the ophiolite units (Fig. 2) but opening out to form broader valleys in the Neogene sediments of the basin floor. Note that these valleys reach far to the NW, with the drainage divide being up to 24 km from the confluence with the River Asi (Fig. 3A). By contrast, streams draining the southeastern flank of the basin are shorter by 60-80% and have far fewer tributaries. Additionally, the drainage divide is much nearer to the SE margin of the graben (typical distance 4-8 km; Fig. 3) than it is on the northern flank. The result of this asymmetry is that much of the mountainous area to the SE of the graben is actually drained by rivers flowing NE, joining the River Asi on or near the Amik plain (Fig. 3) and implying that some water courses have changed their initial orientation by > 180° in < 20 km.

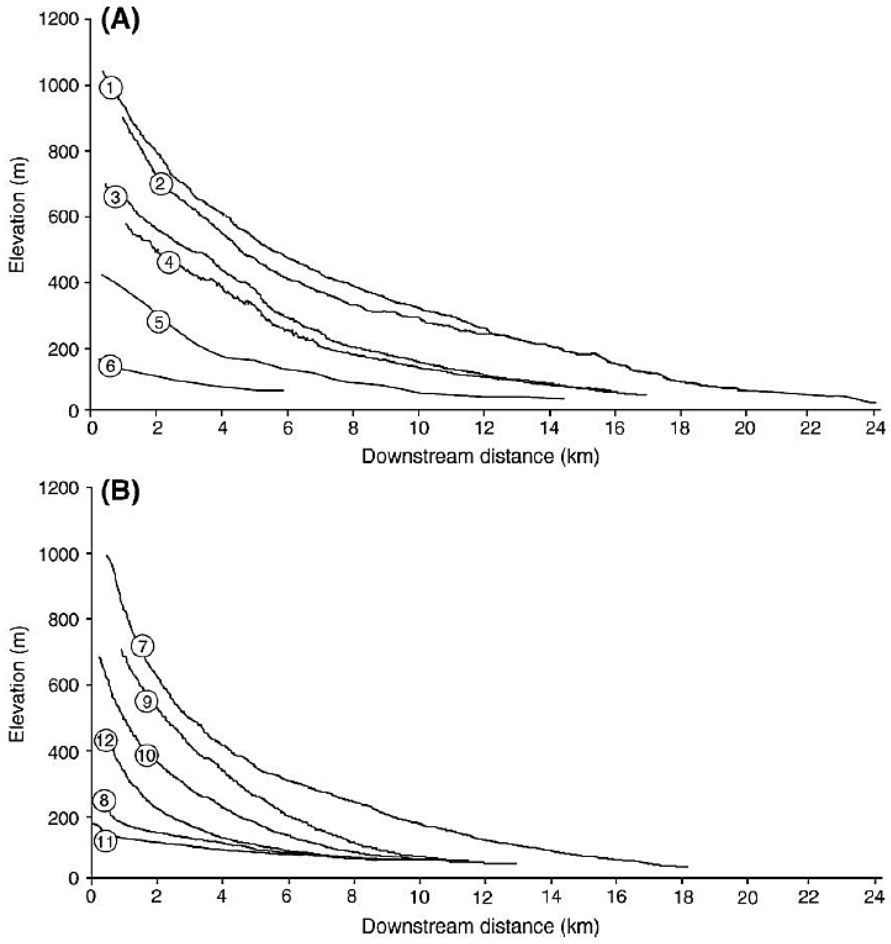

Figure 7. Long profiles of rivers crossing the northern margin of the Hatay graben. (A) shows channels 1-6 and (B) shows channels 7-12. Geographical locality of rivers is shown in Fig. 3B.

Of the larger streams entering directly into the graben, many appear to take a course between mapped fault segments. For example, the Karanlık Dere (Fig. 6A; River 31, Fig. 3B), a 13 km-long river with a drainage area of 40 km^2 cuts between fault segments in two places downstream (between faults α and β; γ and δ). Other large streams to enter the graben at the end of fault segments include rivers 23, 24, and 25, draining a mapped fault-offset south of Antakya (Fig. 3B). Streams with drainage areas > 10 km^2 cutting directly across the faults are relatively rare; examples include river 29 (Fig. 6A) and river 21 (Fig. 6B), an 8-km-long stream that cuts through the footwall of fault κ via a narrow gorge (< 10 m wide) incised into the Eocene bedrock. However, even here, some of the drainage apparently has already been captured by tributaries to river 21 and by river 20, excavating Neogene sediments between faults κ and λ (shown by star, Fig. 6B), which drains through an apparent fault splay farther to the north.

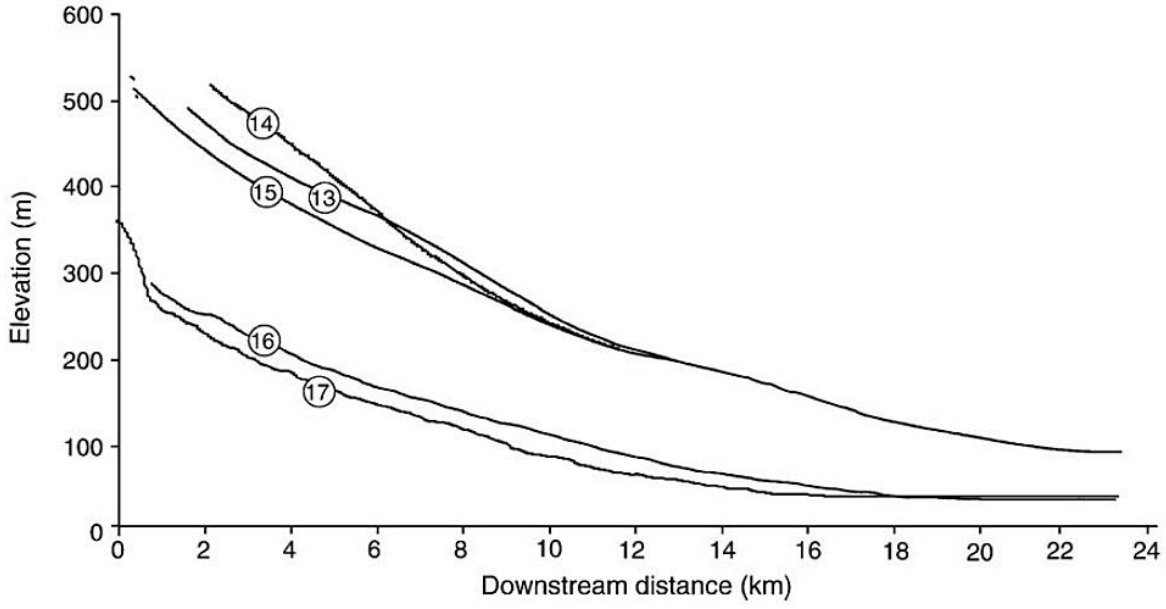

Figure 8 Long profiles of rivers 13-17, draining the southern margin of the Hatay Graben toward the Amik plain. Geographical locality of rivers is shown in Fig. 3B.

4.2. Long profile analysis of tributaries draining into the Hatay Graben

River	L (m)	A (km^2)	θ	k_s	k_{sn}
1	24,000	100	0.73	3400	298
2	24,000	100	0.84	10,781	324
3	15,800	39.5	0.84	6240	399
4	12,350	39.5	0.61	2112	381
5	8700	9.1	0.55	360	200
6	6100	7.1	0.44	40	179
7	16,600	37.4	1	22,800	363
8	8800	8.2	0.57	490	128
9	11,200	13.2	0.64	8772	442
10	9700	10.3	0.8	5640	485
11	5100	6.2	0.51	204	195
12	9300	9.7	0.93	2375	279
13	23,500	125.5	0.54	157	96
14	23,000	146	0.78	4540	71
15	230,000	146	0.64	1572	122
16	19,500	56.7	0.48	21.9	101
17	18,500	56.7	0.7	2820	109
18	9800	9.9	0.59	146	35
19	7900	9.8			
20	5400	6.3			
21	8300	10.2			
22	5300	6.9			
23	9000	12.8			
24	7600	9.8			
25	7100	14.8			
26	10,100	14.8			
27	5200	8.1			
28	4200	5			
29	6200	13.6			
30	5800	8.3			
31	13,100	29.2			
32	9800	16.1			
33	5800	6.4			
34	5100	5.9			
35	5700	11.2			
36	8400	17.7	0.52	202	148

Table 1. Downstream distance, L, drainage area, A, profile convexity, θ, steepness index, ks, and normalised steepness index, ksn, for the rivers shown in Fig. 3, as measured to the Asi river (or the sea).

The long profiles of tributaries draining the northern margin (rivers 1-12; Fig. 3B) of the Hatay Graben are shown in Fig. 7. Dominantly, these profiles are smooth and concave-up: small profile convexities in rivers 3 and 4 at ~ 5 km downstream coincide with the change from ophiolite to Neogene sediments (Fig. 2). Concavities of these channels (Table 1) range from 0.5 to 1, and no discernable trend was found in normalised steepness index along the margin from SW to NE (excluding small channels 6 and 8, which only drain the neogene basin sediments k_{sn} = 336 ± 96).

These long profiles are also similar to channels draining to the Amik plain from the SE side of the graben (rivers 13-17; Fig. 8); these channels also have concave-up long profiles and similar concavities (0.48 < θ < 0.78), although normalised steepness indices are lower. However, the contrast in geometry is huge when we compare these rivers to those draining directly into the Hatay basin from the southern bounding mountains. Channels have substantial profile convexities (Figs. 9A, B) with channel gradients often > 10% in many downstream reaches. These profile convexities reach vertical heights of > 400 m (when measured from the inner graben boundary to the break in slope above the convexity) in several places (e.g., rivers 25, 26 and 32, 34) and are typically upstream of mapped fault segments (Figs. 2, 3A; white bar, Fig. 9).

We also note that rivers appearing to drain between fault segments also display similar convex reaches: all the examples in section 4.1 (see also Fig. 6) have profile convexities that range from

150 to > 400 m, and it seems difficult to distinguish rivers draining across mapped fault segments from those draining through "relay zones" on the basis of their long profile geometry.

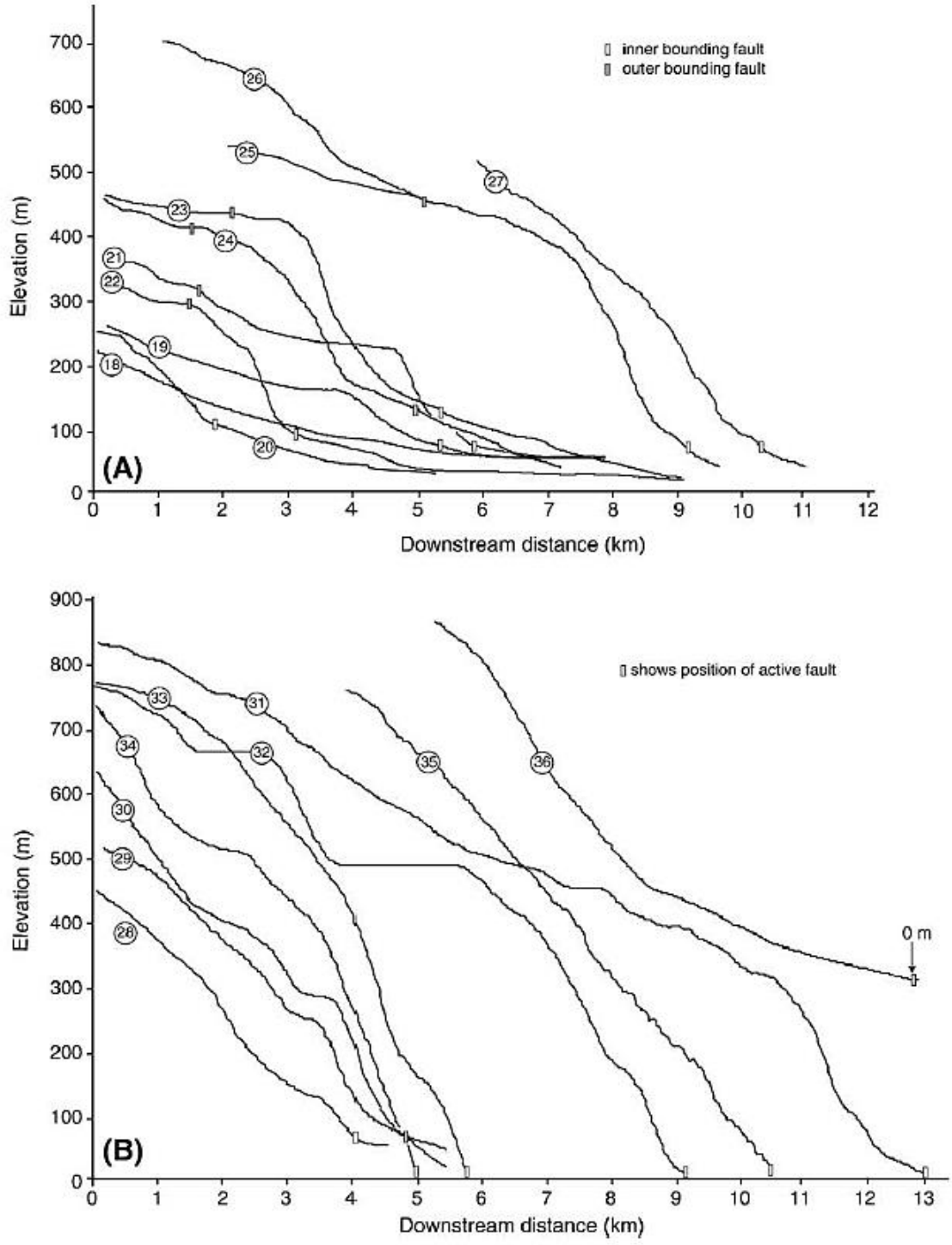

Figure 9. Long profiles of rivers draining NW from the southern margin of the Hatay Graben directly into the basin. (A) shows rivers 18-27 and (B) shows rivers 28-36. Note that for clarity of presentation, rivers 27, 35, and 36 have been shifted along the x axis, and that river 36 is displaced vertically by 350 m, with sea level for this channel shown separately. Position of the innermost bounding fault is shown by a white rectangle, and the outermost fault by a grey rectangle in each profile. Geographical locality of rivers is shown in Fig. 3B.

Importantly, we also note that elevation of long profile convexities varies along strike for the fault array (Fig. 10). Rivers 18 and 36 at the NE and SW ends of the array, respectively, appear to have concave longitudinal profiles (θ = 0.59, 0.52, respectively) with no convex reaches, similar to those in Figs. 7 and 8, while still traversing identical rock types to rivers 19-35. As we head SW along the strike of the Hatay Graben, the size and height of the profile convexities grows, reaching an initial maximum for rivers 25 and 26, despite the fact these rivers apparently drain around an offset in the fault. However, the size of convex reaches is then reduced for the next 10 km along strike, with a minimum at ~ 20 km, where river 28 has a convex reach ~ 100 m in height. We note that this zone of small profile convexities is located in the footwall of the mapped Samandağ fault block, which is currently being incised by the axial river (Figs. 2, 3, 4). From river 31 onward, convex reach elevations increase rapidly, with elevations of 500 m or more typical of channels draining directly into the sea from the steep topography bounding the coast. In particular, river 33 is steeply convex almost all the way to the headwaters. However, ~ 10 km farther along strike, concave-up long profiles are regained (river 36).

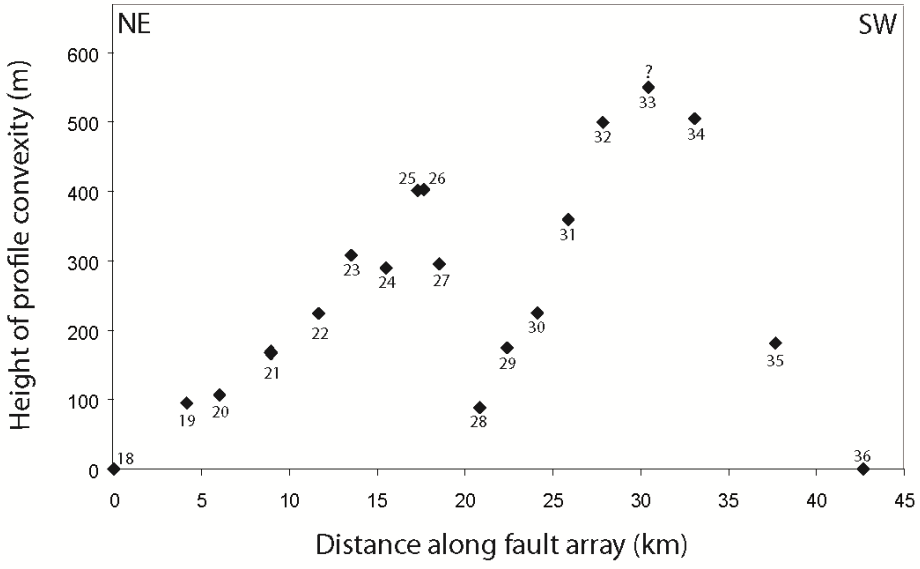

Figure 10 Vertical elevation of long profile convexities for rivers 18-36, as a function of distance along strike of the southern margin of the Hatay Graben from NE to SW. The vertical elevation of these convexities is measured from the innermost active fault segment bounding the southern edge of the basin to the prominent break in slope in the long profile (i.e., where the rate of change of slope is a maximum). For channels where there is more than one slope break upstream, or a gradual change in slope (compare river 21 with rivers 25/26) we use error bars to indicate the range of values for the vertical height of the covnex reach. In a few

cases (e.g., river 29) where the precise position of the present-day active fault is inferred, we use the mapped geological boundary of the graben (Fig. 2), separating basin-fill from uplifted footwall, as a proxy for this. River 33 is convex almost to the headwaters.

Typically, these profile convexities are also correlated with substantial hillslope rejuvenation. Transects through valleys in the gently sloping headwaters of channels (such as rivers 21, 22, 26, and 31) are open and bowl-shaped (black lines, Fig. 11). By contrast, within the convex reaches, valleys are predominantly narrow and "v"-shaped, with hillslope angles approaching 30° (dashed lines, Fig. 11; see also Fig. 4C). We note that the changeover between these two domains typically occurs near or at the break in slope at the top of the long profile convexity.

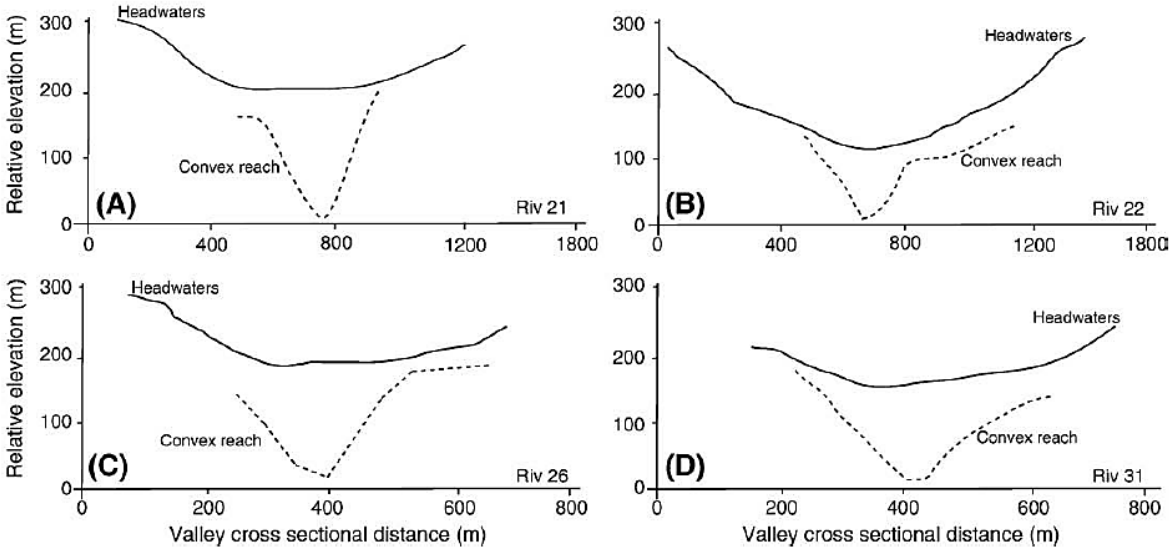

Figure 11 Valley cross sections measured perpendicular to the river for the headwaters (black line) and within the downstream convex reach (dashed line) for (A) river 21, (B) river 22, (C) river 26, and (D) river 31.

4.3. Wind gaps

Wind gaps (dry palaeo-valleys that represent now-abandoned water courses) record drainage reversal events (Keller et al., 1999; Burbank and Anderson, 2001). They have been frequently documented in normal fault-bounded terrains where ongoing tectonic uplift at a point downstream leads to progressive loss or defeat of the upper part of the catchment (e.g., Burbank et al., 1996;

Goldsworthy and Jackson, 2000; Whittaker et al., 2007b). We observe a number of locations in the southern part of the Hatay area where dry valleys in the footwalls of the normal faults bounding the southern edge of the graben can be observed (e.g., SE of fault δ, Fig 6A; and E of fault λ, Fig 6B).

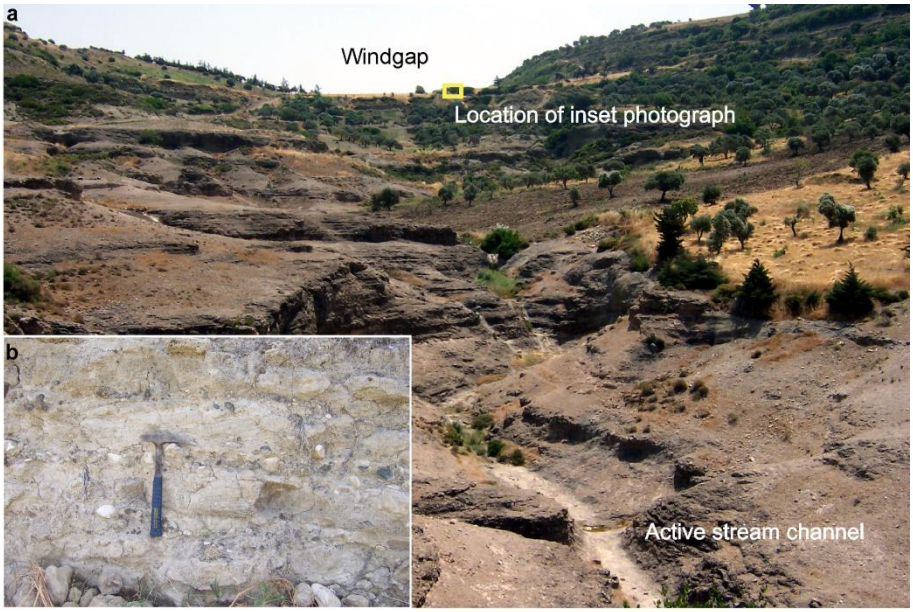

Figure 12. (A) Photograph of wind gap at X (Fig. 6); the stream in the foreground is the headwater of stream 20. (B) Inset shows fluvial conglomerates and cross-bedded sandstones observed to be infilling the wind gap.

In each of these cases, the dry V-shaped depressions in the surrounding topography link to active valleys with streams flowing in opposite directions, suggesting these may indeed be carved by now-defeated channels. These features are most abundant along the drainage divides upstream of faults δ and λ, which form the outer fault boundary of the Hatay Graben. Field investigation of these dry valleys verifies this hypothesis; for example at point *X* (Fig. 6B), we identify a poorly consolidated conglomerate (Fig. 12B) that fines upwards into parallel bedded sands, which infills the dry valley (Fig. 12A). These sediments appear to be incised into the surrounding Miocene sediments, while the active part of the present-day channel has its headwaters to the west and flows to the NW. We therefore interpret this to be a palaeochannel deposit, recording a time when streams in this area flowed to the west, directly across valley-bounding fault λ. In general, the streams showing reversed drainage have the reversed element of the river flowing dominantly to the NE (Fig. 2), while the remainder of the misfit fore-shortened channels flows westward into the Hatay Graben. In the

north, near Antakya, wind gaps are generally orientated E-W, whereas farther to the south the wind gaps are more often orientated NW-SE, neatly reflecting the difference in the fault strike.

Additional evidence for drainage reversal events can be observed at *Y* (Fig. 6A). Here an internally drained basin, sourced by several ephemeral streams, is located behind a southeastward dipping normal fault, labelled ε (Fig. 6A), which is apparently antithetic to fault γ. Sedimentary analyses of the deposits on the basin floor suggest this is a dry lake bed, argued to be Quaternary in age (Boulton, 2006). A wind gap at point Z indicates that the old drainage was blocked by ongoing uplift on fault ε, beheading the channel that once drained into river 32 (Fig. 3B). Notably, this internal basin has not yet been captured by neighbouring channels. This makes it similar to young, normal fault-bounded, internally drained basins found, for example, in the Italian Apennines (e.g., Piano di Peccore on the Irpinia fault; Papanikolaou and Roberts, 2006).

5. Interpretation

5.1. Neotectonics – which faults are active?

Although the north of the graben is topographically higher than the south (Fig. 3) and bordered by mountains that reach > 1600 m in altitude, little evidence is apparent for any substantial dip-slip movement on faults that have been argued by some workers to bound this part of the Hatay Graben (e.g., Yürür and Chorowicz, 1998; Tatar et al., 2004). Structural mapping and sedimentary logging have provided no field evidence for the presence of such a basin-scale fault along the northern graben margin (Boulton et al., 2006); instead Lower to Upper Miocene sediments are observed to progressively onlap the ophiolitic basement along an erosive, conformable contact observed in several river and road sections. Upward from the basal contact, the sedimentary sequence again shows no evidence for a major boundary fault. These observations are supported by the geomorphology: streams draining this side of the Hatay Graben are long, with well-developed

tributary systems typical of equilibrium rivers that have reached topographic steady-state (e.g., Whipple and Tucker, 2002; Whittaker et al., 2007b). Additionally, they display concave-up longitudinal profiles, little variation in normalised steepness index along strike, and no significant perturbation where they cross the postulated fault (Fig. 3). Furthermore, no wind gaps have been documented in this area, and the drainage divide for the basin passively follows the ridge crest of the mountains bounding the graben to the north. However, we note that profile concavities (Table 1) are, on average (~ 0.68), larger than oft-quoted "typical" values of 0.5, but still within the range commonly found by other workers (c.f. Kirby and Whipple, 2001; Duvall et al., 2004; Whipple, 2004 amongst many others). An increase in concavity values are explainable at topographic steady-state if the rate of base-level fall increases downstream, which is what we would expect for these channels if the southern margin of the graben is active (see below). Hence, the rivers flow toward the locus of maximum accommodation generation in the hanging wall.

This synthesis of structural and geomorphic evidence suggests that the northern margin of the graben is tectonically quiescent, and previous interpretations for major faults on the northern margin (e.g., Yürür and Chorowicz, 1998) are without foundation. In contrast, the southern margin of the graben is characterised by short, steep catchments (Fig. 3A) with prominent long profile convexities upstream of mapped graben-bounding faults (Fig. 9), and the presence of several well-documented wind gaps suggesting that northerly directed rivers have been foreshortened through time. Moreover, the axial river drains close to the southern margin of the basin, while much of the area behind the southern-bounding Zıyaret Dağı mountains is now drained by rivers running to the north and east, entering the River Asi near the Amik plain. This geometry means the drainage divide on the southern edge of the basin appears to have migrated toward the basin margin since the Pliocene. Such qualitative observations are typically reproduced by both theoretical and modelling studies of river response to ongoing normal faulting (e.g., Leeder and Jackson, 1993; Cowie et al., 2006).

Such an interpretation is strongly supported by the documented presence and distribution of long profile convexities. For rivers at or close to the detachment-limited end-member (i.e., bedrock rivers), substantial convex or "over-steepened" reaches develop in response to a relative change in uplift rate; for example, through base-level fall, fault initiation, or slip rate increase on pre-existing fault segments (Whipple and Tucker, 2002; Whittaker et al., 2007a) (section 1). In each of these cases, a transient wave of incisional rejuvenation migrates up through the river system as the channel steepens to increase its erosive power to match the new uplift rate. The break in slope above the convex reach represents the boundary between the part of the catchment that has or is adjusting to the "new" uplift rate, compared to the part of the channel that is yet to feel the effects of the relative base-level change (Whipple and Tucker, 2002). For a set convexity migration rate upstream, the vertical elevation of the convex reach is also a positive function of the magnitude of the slip rate perturbation, and the time since it developed (Niemann et al., 2001; Whipple, 2001; Whittaker et al., 2008; Attal et al., 2008). If the transient incisional wave reaches the top of the profile, (or alternatively, if the headwaters are defeated by ongoing fault uplift), a concave-up profile can be regained — although recent field examples from Italy show that this process can take longer than 1 My (Whittaker et al., 2007b, 2008). Therefore, the long-profile convexities, which are ubiquitous on streams draining the southern edge of the graben, are interpreted as evidence that the rivers are undergoing a transient response to ongoing active faulting on the innermost bounding faults of the Hatay Graben. This interpretation is consistent with the fact that these channels also show many of the associated diagnostic features of a transient response to tectonics (see Fig. 17 in Whittaker et al., 2007b), such as narrow valley widths in the transient reaches with hill-slopes rejuvenated to the angle of repose, headwaters with low channel slopes, and drainage divides close to the active fault. These convex reaches are an unlikely result of lithology or external base-level fall. Lithological boundaries (Fig. 2) do not appear to match well with the breaks in slope in the convex reaches; channels at both ends of the fault array do not have long-profile convexities despite traversing similar rock types. Envisaging how an externally driven base-level fall would produce

the characteristic distribution of convex reach heights mapped along strike is also difficult. This is because a base-level fall in the River Asi would have maximum amplitude near the southwestern end of the Hatay Graben and would decay upstream; it would not produce convex reaches with large elevations half way along the valleys that die out at both ends.

The wide range of geomorphic evidence presented above means that the Hatay basin is best interpreted as an asymmetric half-graben, which is bounded by an active normal fault running along the southeastern margin of the basin. This interpretation is also consistent with the position of the River Asi, which therefore occupies the locus of maximum hanging wall subsidence within the valley (c.f., Leeder and Jackson, 1993). We also argue that the Samandağ fault, which bounds the Samandağ Mountain on its northern flank (Figs. 2, 3), is an active structure. This fault has a clear topographic expression, displays triangular facets on the north-facing slope, and has an apparent fault scarp at several points along the slope break (Boulton, 2006). Moreover, the River Asi flows through a steep knickzone and associated gorge in the footwall of this structure (Fig. 5), despite the large drainage area at this point (> 30 000 km^2). Given that the Samandağ fault clearly steps out toward the basin axis and the fact that it significantly perturbs the axial river, an obvious interpretation is that it initiated after the River Asi became established in the hanging wall of the southerly graben margin faults.

However, the basin is also bounded by a second set of mapped normal faults (Fig. 2), which run parallel to the innermost bounding set (e.g., faults γ, δ, λ; Fig. 6). These faults are thought to have initiated during the Middle Miocene (Boulton et al., 2006) and clearly are associated with several sets of wind gaps, demonstrating that uplift on these faults was sufficient to defeat many of the smaller channels that used to drain directly across them. However, we suspect that these faults are not active at the present day. Firstly, rivers 21-26 and 31, which flow across both sets of faults, only display significant convex reaches (i.e., several hundred metres) upstream of the inner-bounding fault near the axial river. Where they cross the outer fault set (shown by grey bars; Fig. 9) there is either little change of slope just upstream of this (e.g., rivers 22, 23, 24, 25), or alternatively

very small profile convexities near the headwaters (e.g., rivers 21, 22). Given the small drainage area and hence stream power of these upstream channel segments, significant continued slip on these faults might be expected to generate a vertically significant knickzones, which we do not see. This means that there is likely no-ongoing transient response to fault activity, which is obviously easily explained if the faults are inactive. However, this could, theoretically, also be resolved if the upper portions of these rivers had completely adjusted to continued uplift on the outer-bounding fault set despite their small drainage area (i.e., the channels had reached topographic steady-state with respect to the long-term uplift field). This could be achieved if they maximised their incision capacity by gorge formation or channel narrowing, rather than by streamwise gradient changes, as has been documented in other steady-state rivers crossing normal faults over time periods > 3×10^6 years, albeit with much larger discharges (Whittaker et al., 2007b). However, field evidence argues against this interpretation. The upper parts of rivers crossing these faults (such as river 31) appear to have wide open valleys in the headwaters (see Fig. 11C), which would not be expected if the channel had regained a concave-up profile, but had narrowed valley widths to enable the river to keep pace with ongoing fault uplift. Additionally, these faults have much less present-day topographic expression than the inner faults; and field investigation shows that the remnants of the fault planes are completely degraded, unlike the innermost bounding fault set. Therefore, we interpret the outermost bounding faults to be presently inactive.

5.2. Fault development, lengths and slip rates

5.2.1. Fault evolution and size

The fact that rivers crossing apparent fault offsets and relay zones (Fig. 6) along the strike of the southern inner-bounding fault all display large convex reaches, as well as those crossing mapped fault segments, is particularly significant. The clear interpretation is that although some rivers, such as 25 and 31 etc., originally drained *between* short fault segments on the inner-bounding faults of the graben, as is typically seen in extensional terrains (c.f., Leeder and Jackson, 1993; Cowie et al.,

2006), these rivers are now being perturbed by tectonic uplift. The simplest explanation for these observations is that the rivers are responding transiently to fault uplift because the once separate fault segments bounding the southern margin of the Hatay Graben have become linked. Such an event would produce substantial convex reaches as the rivers adjust to the new uplift rate imposed on the channel. Moreover, this effect has been documented both in numerical studies of river response to fault growth and interaction (e.g., Cowie et al., 2006; Attal et al., 2008) and also for field examples in Italy, Greece, and the canyon lands of Utah (Cowie and Roberts, 2001; Commins et al., 2005; Whittaker et al., 2008; Cowie et al., 2008). In all these examples, the evidence is excellent that fault linkage has occurred and has perturbed channels draining through former fault offsets. We also note that fault growth and interaction is typically associated with (i) an increase in slip rate along the strike of the whole array, but particularly toward the middle of newly linked fault segments, because the central faults find themselves under displaced for the longer structure of which they now form a part and (ii) the "switching off" of distal fault segments that run parallel to the linked fault if the total rate of extension across the graben is to remain the same (McLeod et al., 2000; Cowie and Roberts, 2001; Roberts and Michetti, 2004).

We believe that the Hatay area provides good evidence of this process. No evidence is available for current activity on the outermost faults bounding the graben, whilst we have documented that these faults were active in the past, suggesting these faults have now "switched off." Moreover, all the channels draining across the inner-bounding faults of the graben display convex reaches that vary *systematically* along strike. This is important because rivers crossing pre-existing fault segments that became subaerial by the Pliocene, *but had not changed their slip rate since that time,* might be expected to either:

(i) have been defeated in the 5 million years available (something that has clearly happened to channels draining the outermost graben-bounding faults given the documented wind gaps);

(ii) have reached topographic steady-state with concave-up profiles [documented response times are ~ 1-2 x 10^6 My for channels with similar drainage areas, and lithologies and a comparable Mediterranean climate (Whittaker et al., 2007b)]; or

(iii) display anomalously high convex reach heights compared to rivers nearby that were perturbed more recently, representing the additional time available for the profile convexity to grow and to migrate upstream.

As we make none of these observations, we argue that a far simpler and cogent explanation is that all the channels are simultaneously responding to fault slip rate acceleration as a result of fault interaction and linkage along the array. In this interpretation, we would expect vertical height of long-profile convexities to mirror the throw rate increase along the fault — i.e., low or absent at the ends of the fault, and largest for rivers cutting across the centre of linked fault segments (Whittaker et al., 2008). In fact, along the southern margin of the Hatay Graben, we document two peaks in convex reach heights (Fig. 10) at ~ 15 and 30 km along strike. Moreover, the significant minimum in convexity heights at ~ 20-25 km along the array (for rivers 28-30) coincides with the position of the Samandağ fault, which runs parallel to the southern margin but has stepped out into the basin. Therefore, any continuation of the basin-bounding faults is in the stress shadow of the Samandağ fault in this area, depressing the throw rate on the former. This geometry is well known in other areas such as around the Fucino fault, Italy (Roberts and Michetti, 2004). The faults probably join at a shallow level in the crust, and therefore the total throw rate across the overlapping strands can be taken cumulatively. This geomorphic analysis suggests that the Hatay Graben is bounded along its southern margin by at most three fault strands: one linking from 0-25 km along strike (starting from the north), another from 25-40 km along strike, and additionally, the Samandağ fault that runs parallel to the zone where the former meet. However, given the significant topographic expression and geomorphic impact of this latter structure and the relatively large throw it has accumulated (> 500 m) for a segment that is apparently only 6.5 km long, the Hatay Graben is now quite conceivably bounded by a soft-linked active normal fault (the Antakya fault) that is > 40

km in length and runs along the entire southern margin of the graben. This finding has substantial hazard implications for the area (see section 5.4).

5.2.2. Estimating fault slip rates

These results evidently raise questions about the timing of fault linkage and acceleration and about the present day slip rate on the fault. Clearly, a minimum slip rate for parts of the basin-bounding fault can be deduced by dividing the total amount of throw accumulated since the early Pliocene by the time available. For the northern end of the array near the city of Antakya, this calculation (1000 m / 5 My) gives time-averaged rates of up to 0.2 mm/y for this part of the fault. However, this figure does not take into account any increase in slip rate through time, for which we provide evidence above. However, an estimate of the relative slip rate enhancement factor, E, along a linking fault array can be calculated from the length of the pre-existing fault segments, L_i ,and the distance from the midpoint of the i -th segment to the nearest tip of the newly linked fault, R_i ,(Cowie and Roberts, 2001). For a simple triangular displacement profile, this is calculated as:

$$E = 2\,(R_i/L_i) \qquad (2)$$

Detailed geological mapping (Fig. 2; see also Boulton et al., 2006; Boulton and Robertson, 2007) suggests that the fault segments that divide relay ramps and transfer zones are ~ 5 km long. From the evidence presented above we can (to first order) model the rivers draining the SE margin of the Hatay basin as crossing two linked arrays, each up to 25 km long (note that apart from the main axial river none of these channels traverse the Samandağ fault). Assuming the constituent fault segments linked at approximately the same time, we can therefore predict the slip rate enhancement along strike (Fig. 13). In this case, central parts of both the NE and SW faults underwent a slip rate increase of up to 5 times upon linkage, with a throw rate minimum at the centrally located segment tips, 20-25 km along strike. If, at a subsequent time, these two 25-km-long faults have became soft-linked via the basin-stepping Samandağ fault, Eq.2 suggests that this 6.5-km-long structure could have slip rates up to 7 times greater than the initial slip rate for segment 5, which runs

approximately parallel. However, throw rate detected by rivers crossing the middle parts of the two 25-km-long fault strands would show little additional enhancement [i.e., for segment 3 (Fig. 13), we predict E = (2 x 12.5) / 25, i.e., no throw rate enhancement].

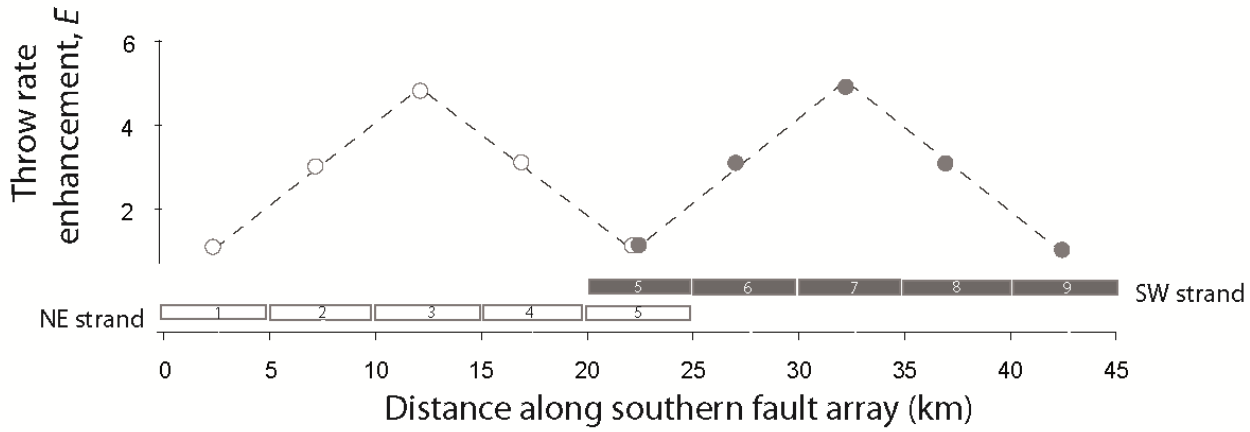

Figure 13. Estimates of throw rate enhancement factor, E, for two linked 25-km-long fault strands, segmented in 5 km intervals, running along the NE (white circles) and SW (grey circles) of the southern margin of the Hatay basin.

To first order, the twin-peaked distribution of transient profile convexities along strike (Fig. 10) roughly matches the acceleration calculation shown in Fig. 13. In particular, we document that convex reach heights vary by ~ 4 times between 5-15 km along strike from the NE, which is very similar to the throw rate enhancement predicted between strand 1 and 3 in Fig. 13A. Similar arguments apply for the SW strand of the bounding fault. Clearly, the peak in convex reach heights for the northern strand is somewhat asymmetric along strike (maximum at 16 km); but as small deviations from a geometrically "ideal" distribution of throw and throw rate are common (see Roberts and Michetti, 2004; Commins et al., 2005) and convex reach heights are evidently not an exact proxy for fault slip rate [see Whittaker et al. (2008) for more discussion] we do not find this unexpected. For channels near Antakya (e.g., rivers 23-27; ~ 15 km along strike) where we have the best constraints on the throw of the faults [~ 1000 m (section 2; Boulton, 2006)] this analysis suggests that they have likely seen a throw rate increase of a factor of 4-5.

Assuming this throw rate increase is a product of a single linkage event, we can express the total throw, D, since the Early Pliocene at any point along strike as

$$D = r_1 t_1 + r_2 t_2 \qquad (3)$$

where r_1, r_2 are the throw rates before and after the linkage event, respectively; t_1 is the time between fault initiation and fault linkage; t_2 is the time after the slip rate increase. Therefore, $t_1 + t_2 = 5$ My and $r_2 = Er_1$. Given an estimate of D, we can therefore constrain the range of times that a single slip rate increase could have occurred and the respective absolute slip rates that date would imply. This is computed in Fig. 14 for the vicinity of rivers 23-27, where D is ~ 1000 m, and the throw rate enhancement, E, is a factor of 4-5. For any given time since the slip rate acceleration in the past, t_2, we can thus estimate the throw rate before acceleration (squares) and the throw rate afterward (circles). Note that for comparative purposes we also show r_2 predictions for $E = 5$; $D = 1050$ m, and $E = 4$; 950 m respectively (lines) — these form the upper and lower bounds, respectively. r_1 predictions for fault displacements of 1000 ± 50 m lie within the squares shown.

However, the throw rate on the fault post acceleration, r_2, should also be independently consistent with the time taken to grow a long-profile convexity measured on a river at that point. For channels close to the detachment-limited end member and crossing active faults, Whittaker et al. (2008) showed both theoretically and through modelling work that the vertical convexity height, H_3 should scale directly with the throw rate perturbation. For our purposes, this means that $H = t_2(r_2-r_1)$. Maximum convexity heights for rivers on the NE part of the southern bounding fault are ~ 400 m and, additionally, the thickness of Plio-Pleistocene sediments in the basin (section 2) is ≥ 100 m. This means we need to account for 500 ± 50 m of slip near the centre of the NE fault strand since the fault linkage event. Using this additional constraint, we can therefore estimate both the timing of fault linkage and also predict the current slip rate on the fault. For fault acceleration times < 1 My, clearly we would need a slip rate to generate the profile convexity $r_{(\text{knickzone})}$ (triangles, Fig. 14) that is much higher than the predicted post-acceleration throw-rate, r_2 (circles). The opposite is true for fault acceleration occurring before 2 Ma. Our results show the best fit is for fault linkage

and slip rate increase at ~ 1.4 ± 0.2 Ma, implying a current slip rate on this part of the fault of 0.45 ± 0.05 mm/yr with slip rates of ~ 0.1 mm/yr prior to this point in time. Profile convexities for the SE strand (e.g., river 34) produce almost identical results — *H* as directly measured is larger (~ 500 m), but as sediment is not stored in the hanging wall, the total amount of slip to be accommodated is similar.

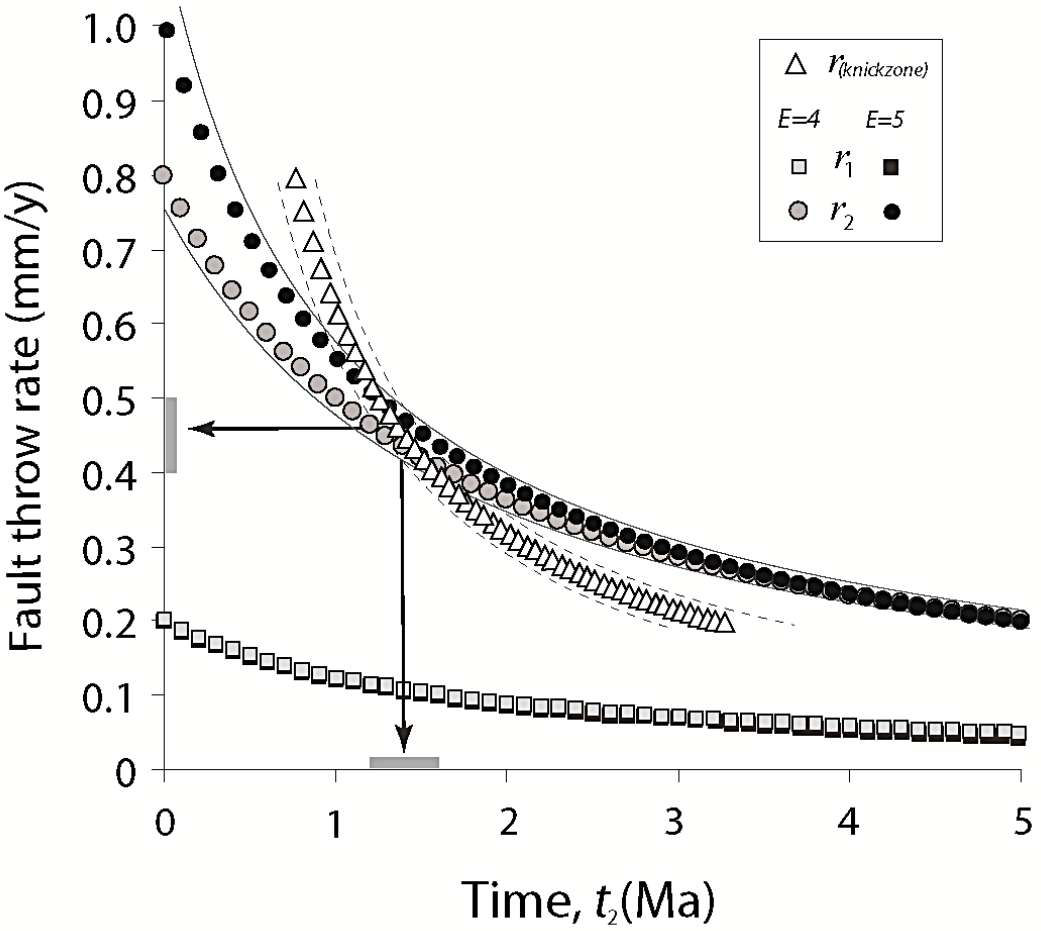

Figure 14. Calculation of possible slip rates for the central part of the NE fault strand before and after fault linkage as predicted by Eq. 3. Given a fault displacement of D = 1000 m, squares show required slip rate before fault linkage, r_1, as a function of time since the slip rate increase occurred, t_2; and circles show the rate after linkage, also as a function of t_2. Grey symbols are for a throw rate enhancement factor, E = 4; black symbols are for E = 5. Black lines show variability in r_2 for E = 4; D = 950 m (lower bound) and E = 5; D = 1050 m (upper bound). Triangles show the throw rate, $r_{(knickzone)}$, needed to generate a 500 m high convex reach in a river profile as a function of time. Dashed bounding lines show $r_{(knickzone)}$ for profile convexities of 450 and 550 m, respectively. Assuming a single linkage event, we require $r_{(knickzone)} = r_2$. Arrows and grey bars show best fit occurting at 0.45 ± 0.05 mm/y, implying the fault linkage event occurred at 1.4 ± 0.2 Ma.

The above calculation is evidently an approximation as we assume a single, instantaneous increase in slip rate on the fault as a result of linkage; we have used a uniform fault segment length of 5 km to estimate *E*; and we do not account for any knickzone migration that will serve to increase the vertical elevation of long profile convexities through time. Nevertheless, evidence from the central Apennines suggests that changes in fault slip rate from linkage are very rapid in geological terms (Cowie and Roberts, 2001; Roberts and Michetti, 2004), while fault segment lengths in the Hatay area are unlikely to be significantly different from the value used.

Importantly, a comparison of the rate derived above to other methods of calculating uplift rates is favourable. For example, radiocarbon dating of uplifted marine terraces identified on the southern coastal margins of the graben indicate that the region has been uplifting at ~ 0.55 mm/yr for the last 5000 years (Pirazzoli et al., 1991; Erol and Pirazzoli, 1992). Therefore, this analysis demonstrates that it is now possible to derive well-constrained estimates of both fault-slip rates and the temporal evolution of fault arrays from geomorphic data.

5.3. Structural evolution of the area

The detailed observations and new tectonic constraints allow us to build upon previous models for the evolution of the Hatay Graben in order to develop a sophisticated understanding of the tectonic evolution of the area (Fig. 15). Syn-sedimentary relationships indicate that normal faulting in the Hatay Graben was active during the Middle and Late Miocene (Boulton et al., 2006; Boulton and Robertson, 2008), although relatively high sea level and high rates of sedimentation meant these faults had little topographic expression (Boulton et al., 2006) (Fig. 15A). Faulting is inferred to be the result of far field stresses related to continental collision to the north resulting in flexural, regional subsidence (Boulton and Robertson, 2008). Stratigraphic offsets indicate ~ 500 m of throw on initial basin-bounding faults from the base of the Upper Miocene (11 Ma) to the early Pliocene (~ 5 Ma), suggesting slip rates of ~ 0.1 mm/yr for this time period. A drainage network in the area

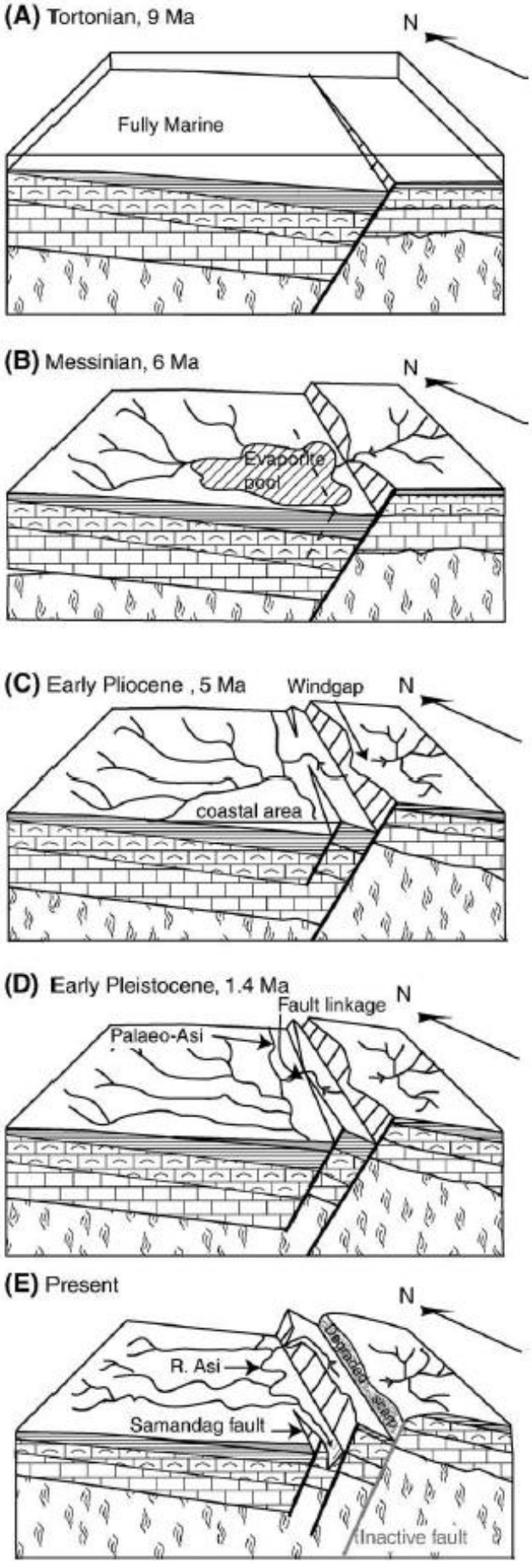

developed after the onset of a regional regression during the Messinian, associated with the well-documented salinity crisis (Fig. 15B). During this time, erosional surfaces formed on the graben flanks and evaporites were deposited in the axial zone attesting to a change in graben dynamics (Boulton, 2006). River systems likely did not switch on until the later part of this period when regional evidence suggests that the climate became wetter at about 5.8 Ma (Griffin, 2002).

Pliocene and younger sediments are confined to the axial zone of the graben, whereas Messinian evaporites are also present in subbasins on the graben flanks (Boulton et al., 2006). This implies that the innermost faults

Figure 15. Simplified block diagrams illustrating the fault evolution of the graben. (A) Late Miocene (Tortonian); a relative sea level high, normal faulting begins to result in syn-sedimentary thickening into the fault zone but topography is still subdued. (B) Late Miocene (Messinian); the Messinian salinity crisis, low sea level and evaporite deposition within the basin and initial development of a river system, increased topographic expression of fault zone. (C) Pliocene; inner fault relay becomes active, graben increasingly well defined with corresponding effect on river evolution, although the graben floor is partly marine at this time. (D) Early Pleistocene ~1.6 Ma; fault linkage of the inner fault array takes place; around this time or shortly after, the outer fault array becomes inactive. (E) Present day; development of fault zones and river networks into present configuration.

became active or only developed significant topographic expression between the deposition of the Messinian evaporites and the Pliocene sediments, at ~ 5 Ma. During the Pliocene (Fig. 15C), the faults continued to grow and lengthen. As a result, continuing uplift on the flanks of the graben apparently defeated the antecedent stream network near the palaeoridge crests, bringing the drainage divide closer to the forming half graben. By the early Pleistocene, the inner faults began to interact and link (Fig. 15D), resulting in throw rates in the centre of basin-bounding faults increasing to ~ 0.45 mm/yr. This slip rate increase also drove up the flank elevation of the southern margin of the graben and caused footwall incision of graben-draining streams (with concomitant formation of transient knickzones). The outmost fault zone likely became inactive at this time, as all extension in the area became focussed on the inner array (c.f., Cowie and Roberts, 2001). Concomitantly, the palaeo-Asi adopted a position in the proximal hanging wall of the southern bounding faults as accommodation space was generated rapidly here. The Samandağ fault was the last major fault to develop; this fault has stepped out into the graben after the establishment of the course of the River Asi, which has subsequently kept pace with footwall uplift, incising a significiant gorge only a few kilometres upstream of the point of discharge into the sea (Fig. 15E).

Ongoing seismicity (Boulton and Robertson, 2008) and the analysis presented in this paper show that the basin-bounding normal faults continue to be active. However, strike-slip faulting has been increasingly important in the deformation of this area, with high numbers of strike-slip faults recorded in Pliocene sediments (Boulton, 2006; Boulton and Robertson, 2008). This latter observation has led to two contrasting models of graben formation being proposed for this region of Turkey: A two-phase evolution, consisting of an initial phase of extension during the Miocene forming the graben-bounding faults, followed by strike-slip faulting in a second phase, during or after the Pliocene; or alternatively, a model invoking strain-partitioning or "partitioned transtension", where two styles of faulting coexist in different areas; i.e., extensional basin-bounding faults (extension-dominated transtension) versus strike-slip faulting (wrench-dominated transtension) within the graben (Boulton and Robertson, 2008). Our analysis here unequivocally

shows that the graben-bounding normal faults have been active throughout the Plio-Pleistocene to the present day and that strain has not all been transferred onto strike-slip faults in the axial zone of the graben. Therefore, the model of oblique extension through partitioned strain between normal and strike-slip faulting is the most appropriate for this graben.

5.4 Hazard assessment

Seismic hazard is based upon the quantitative estimation of the peak ground shaking at a particular site; therefore, the accurate determination of ground acceleration is of paramount importance for countries such as Turkey, which are situated along major seismic belts. Several attempts have been made at quantifying the level of earthquake risk in Turkey. The present seismic hazard zonation map (published by the Turkish Ministry of Reconstruction and Settlement, 1996) is divided into five subclasses (I-V); however, as Kayabali (2002) and Kayabali and Akin (2003) discussed, a number of major flaws have been noted in this current and official seismic hazard map. This led Kayabali (2002) and Kayabali and Akin (2003) to develop new and more sophisticated hazard maps for Turkey that were based upon the active fault map of Turkey by Saroglu et al. (1992) and the tectonic lineament map of Yaltirak et al. (1998). Unfortunately, these maps do not include 25-40 km long fault(s) bounding the southern margin of the Hatay Graben. As a result, the predicted maximum peak ground acceleration for the area is likely to be far too low, significantly underestimating the hazard in this area.

The construction of a detailed seismic hazard map for this region of Turkey is beyond the scope of this paper, but it is useful to recalculate the potential ground acceleration for the Hatay area, using the deterministic approach to seismic hazard assessment. This requires the calculation of the maximum magnitude of a causative fault and the attenuation of seismic energy away from the fault zone. The maximum magnitude for a fault can be calculated using surface rupture length,

generally considered to be between one half and one third of the total length of the fault (Mark, 1977). Following Wells and Coppersmith (1994), this can be expressed, for a normal fault, as

$$M_w = 4.86 + 1.32\log L \qquad (4)$$

where M_w is moment magnitude; and L is fault rupture length (in km).

Assuming that the Antakya fault is linked for the total 40 km, a rupture along one third to one half of the length would result in an M_w of between 6.3 and 6.6. If the faults are linked to the lower estimate of 25 km, the predicted M_w is reduced slightly, to range between 6.0 and 6.3. If the attenuation relationship of Joyner and Boore (1998) is then used [shown by Kayabali and Akin (2003) to be the most appropriate for Turkish geology] an upper estimate for peak horizontal ground motion of 0.34 g can be calculated for a distance of 10 km away from the fault, which includes most of the Hatay Graben. This value corresponds to the areas of highest seismic hazard as defined by the seismic hazard zoning for Turkey. In addition, we should note that the unconsolidated nature of the graben fill will also act to increase the effect of an earthquake and the effects will be greater than on the graben flanks that are composed of solid bedrock and are less densely populated than the graben floor. Clearly, therefore, recent revisions to the seismic hazard maps of Turkey grossly underestimate the hazard in the Hatay region and must be revised to reflect this.

5.5. Wider Implications

In addition to the implications for the tectonic evolution of the eastern Mediterranean region, this work has a significant generic impact. We have demonstrated that a synthesis of detailed geomorphic observations, in particular river long profile convexities, and pre-existing geological data can be a powerful, quantitative tool for unravelling the active tectonics of extensional basins. This is important because, until recently, attempts to extract tectonics from topography have only met with limited success (c.f., Kirby et al., 2003; Wobus et al., 2006) and have been restricted in applicability to systems that have reached topographic steady state. In contrast, this is one of the

first studies (see also Kirby et al., 2007, 2008) not only to use geomorphological techniques to demonstrate that an area is undergoing a transient response to tectonics, but also to quantify slip rates on basin-bounding faults and to estimate the timing of fault interaction.

In principle, our analysis is applicable to any neotectonic province undergoing a transient response to tectonics. As published estimates of landscape response times to tectonic perturbation are typically of the order of 1-3 My (Whittaker et al., 2007b, 2008), and can be longer (e.g. Clark et al., 2005; Pelletier, 2007), this implies that "young" extensional basins (drained by sediment-starved bedrock catchments) are the most fertile targets for further investigation. Given the number of normal fault-bounded grabens for which some geological and structural data do exist, but where tectonic rates over time periods of ~ 10^6 years are poorly constrained (e.g., much of the Western Anatolian Extensional Province), we believe this approach could be applied widely to many extensional systems.

6. Conclusions

We have combined qualitative inferences drawn from stream network analyses and geological field mapping with quantitative data derived from long profile analyses of streams, to unravel the tectonic evolution of a regionally significant oblique-extensional basin (the Hatay Graben) in southern Turkey. We show that footwall channels crossing basin-bounding faults display transient long-profile convexities that vary along strike, and we interpret these to be a response of the channels to linkage along the fault array. Our data enable us to quantify the present-day slip rates of graben-margin normal faults and the tectonic evolution of the region through time. In particular, we show that from 5 My to ~ 1.4 My, throw rates on the faults were no more than 0.1 mm/y and that post-acceleration at 1.4 Ma, maximum slip rates increased to 0.45 mm/y. We also demonstrate from a synthesis of structural, geological, and geomorphic analyses that despite topography being highest in the north of the graben all the major active normal faults are located on the southeastern boundary and that no evidence was found for active extension along the northwestern margin of the

Hatay Graben. Additionally, our analysis shows the half-graben is now bounded by a soft-linked normal fault, which may be as much as 40 km in length, a finding that has substantial hazard implications for the area.

These findings support previous models of graben formation as an oblique-extensional graben where strain partitioning has occurred, forming part of the diffuse plate boundary between Africa and Anatolia. Moreover, this paper now demonstrates that a synthesis of geomorphological observations with pre-existing geological data can now be successfully used to calculate realistic slip rates on active faults for time periods > 10^6 years.

8. Acknowledgements.

SJB would like to acknowledge NERC award NER/S/A/2002/10361 and a fieldwork grant from the British Society for Geomorphology (formerly the British Geomorphological Research Group). ACW was supported by StatoilHydro and NERC award NER/S/A/2002/10359. The manuscript benefitted from insightful discussion with Patience Cowie and Philip Allen, thoughtful comments on the text from Ann Mather, Martin Stokes, Mikael Attal and Dan Hobley, and positive reviews by Eric Kirby, Nicole Gasparini and an anonymous reviewer. Our thanks to all.

9. References

Arpat, E., Şaroğlu, F., 1972. The East Anatolian Fault System; thoughts on its development. Bulletin of the Mineral Research and Exploration Institute of Turkey 78, 33-39.

Attal, M., Tucker, G.E., Whittaker, A.C., Cowie, P.A., Roberts, G.P., 2008. Modelling fluvial incision and transient landscape evolution: influence of dynamic channel adjustment. Journal of Geophysical Research, 113, F03013, doi:10.1029/2007JF000893.

Barka, A.A., Kadinsky-Cade, C., 1988. Strike-slip geometry in Turkey and its influence on earthquake activity. Tectonics 7, 663-684.

Boulton, S.J., 2006. Tectono-sedimentary evolution of the Hatay Graben (Southern Turkey). Ph.D. thesis, University of Edinburgh, Scotland.

Boulton, S.J., Robertson, A.H.F. 2007. The Miocene of the Hatay area, S Turkey: transition from the Arabian passive margin to an underfilled foreland basin related to closure of the Tethys Ocean. Sedimentary Geology 198, 93-124.

Boulton, S.J., Robertson, A. H. F., 2008. The Neogene-Recent Hatay Graben, South Central Turkey: graben formation in a setting of oblique extension (transtension) related to post-collisional tectonic escape. Geological Magazine. doi:10.1017/S0016756808005013

Boulton, S.J., Robertson, A.H.F., Ünlügenç, U.C., 2006. Tectonic and sedimentary evolution of the Cenozoic Hatay Graben, Southern Turkey: A two-phase, foreland basin then transtensional basin model. In: Robertson, A.H.F., Mountrakis, D. (Eds.), Tectonic Development of the Eastern Mediterranean Region. Special Publication of the Geological Society of London, London, U.K., 260, pp. 613-634.

Boulton, S.J., Robertson, A.H.F., Ellam, R.M., Şafak, Ü., Ünlügenç, U. C., 2007. Strontium isotopic and micropalaeontological dating used to help redefine the stratigraphy of the neotectonic Hatay Graben, southern Turkey. Turkish Journal of Earth Sciences 16, 141-180.

Burbank, D.W., Anderson, R.S. 2001. Tectonic Geomorphology. Blackwell Science, Oxford, U.K, 274 p.

Burbank D.W., Raynolds, R.G.H., Johnson, G.D., 1986. Late Cenozoic tectonics and sedimentation in the north-western Himalayan foredeep: II. Eastern limb of the Northwest Syntaxis and regional synthesis (India, Pakistan). In: Allen, P. A., Homewood, P. (Eds.). Foreland basins. International Association of Sedimentologists Special Publications, Oxford, U.K., 8, pp. 293-306.

Burbank D.W., Meigs, A., Brosovic, N., 1996, Interactions of growing folds and coeval depositional systems. Basin Research 8, 199-223.

Clark, M.K., Gweltaz, M., Saleeby, J., Farley, K.A., 2005. The non-equilibrium landscape of the southern Sierra Nevada, California: GSA Today, 15, p. 4–10.

Commins, D., Gupta, S., Cartwright, J., 2005. Deformed streams reveal growth and linkage of a normal fault array in the Canyonlands graben, Utah. Geology 33, 645-648.

Cowie P.A., Roberts, G.P., 2001. Constraining slip rates and spacings for active normal faults. Journal of Structural Geology 23, 1901-1915.

Cowie, P.A., Attal, M., Tucker, G.E., Whittaker, A.C., Naylor, M., Ganas, A., Roberts G.P., 2006. Investigating the surface process response to fault interaction and linkage using a numerical modelling approach. Basin Research 18, 231-266.

Cowie, P.A., Whittaker A.C., Attal, M., Tucker G.E., Roberts G.P., Ganas, A., 2008. New constraints on sediment-flux dependent river incision: Implications for extracting tectonic signals from river profiles, Geology, 36, 535–538.

Duvall, A., Kirby, E., Burbank, D.W., 2004. Tectonic and lithologic controls on channel profiles and processes in coastal California. Journal of Geophysical Research, 109 (F3), doi: 10.1029/2003JF000086.

Erdik, M., Aydınoğlu, N., Pınar, A., Kalafat, D., 1997. Report of Hatay Earthquake. Kandilli Observatory, Istanbul.

Erol, O., Pirazzoli, P.A., 1992. Seleucia Pieria: an ancient harbour submitted to two successive uplifts. The International Journal of Nautical Archaeology 21 (4), 317-327.

Finnegan, N.J., Roe, G., Montgomery, D. R., Hallet, B., 2005. Controls on the channel width of rivers: implications for modelling fluvial incision of bedrock. Geology 33, 229-232.

Garfunkel, Z., Ben-Avraham, Z., 1996. The structure of the Dead Sea Basin. Tectonophysics 255, 155-176.

Griffin, D.L., 2002. Aridity and humidity: two aspects of the late Miocene climate of North Africa and the Mediterranean. Palaeogeography, Palaeoclimatology, Palaeoecology 182 (1-2), 65-91.

Goldsworthy, M., Jackson, J.A., 2000. Active normal fault propagation in Greece revealed by geomorphology and drainage patterns. Journal of the Geological Society, London, U.K., 157, 967-981.

Jackson, J., 2001. Living with earthquakes: know your faults. Journal of Earthquake Engineering 5, (special issue 1) 5-123.

Jackson, J.A., Norris, R., Youngson, J., 1996. The structural evolution of active fault and fold systems in central Otago, New Zealand: evidence revealed by drainage patterns. Journal of Structural Geology 18, 217-234.

Joyner, W.B., Boore, D.M., 1998. Measurement, characterization, and prediction of strong ground motion. IN: von Thun, J.L. (Ed) Earthquake Engineering and Soil Dynamics: 2. Recent Advances in Ground Motion Evaluation. ASCE, New York, pp 43-102.

Kayabali, K., 2002. Modelling of seismic hazard for Turkey using recent neotectonic data. Engineering Geology 63, 221-232.

Kayabali, K., Akin, M., 2003. Seismic hazard map of Turkey using the deterministic approach. Engineering Geology 69, 127-137.

Keller, E.A., Gurrola, L., Tiernay, T.E., 1999. Geomorphic criteria to determine direction lateral propagation of reverse faulting and folding. Geology 27, 515-518.

Kilic, S., Evrendilek, F., Berberoglu, S., Demirkesen, A.C., 2006. Environmental monitoring of land-use and land-cover changes in a Mediterranean region of Turkey. Environmental Monitoring and Assessment 114, 157-168

Kirby E., Whipple, K.X., 2001. Quantifying differential rock-uplift rates via stream profile analysis. Geological Society of America Bulletin 29, 415-418.

Kirby E., Whipple, K.X., Tang, W., Chen, Z., 2003. Distribution of active rock uplift along the eastern margin of the Tibetan Plateau: inferences from bedrock channel longitudinal profiles. Journal of Geophysical Research 108 (B4), 2217, doi: 10.129/2001JB000861.

Kirby, E., Johnson, C., Furlong, K., Heimsath, A., 2007. Transient channel incision along Bolinas Ridge, California: evidence for differential rock uplift adjacent to the San Andreas Fault. Journal of Geophysical Research 112, F03S07, doi:10.1029/2006JF000559.

Kirby, E., Whipple, K.X., Harkins, N., 2008. Topography reveals seismic hazard. Nature Geoscience 1, 485-437.

Lavé, J., Avouac, J.P., 2001. Fluvial incision and tectonic uplift across the Himalayas of central Nepal. Journal of Geophysical Research, 106, 26561-26591

Leeder, M.R., Jackson, J.A., 1993. The interaction between normal faulting and drainage inactive extensional basins, with examples from the western United States and central Greece. Basin Research 5, 79-102.

Lyberis, N., 1988. Tectonic evolution of the Gulf of Suez and the Gulf of Aqaba. Tectonophysics 153 (1-4), 209-220.

Mark, R.K., 1977. Applications of linear statistical model of earthquake magnitude versus fault length in estimating maximum expectable earthquakes. Geology 5, 464-466.

McClusky, S., Balassanian, S., Barka, A., Demir, C., Ergintav, S., Georgiev, I., Gurkan, O., Hamburger, M., Hurst, K., Kahle, H., Kastens, K., Kekelidze, G., King, R., Kotzev, V., Lenk, O., Mahmoud, S., Mishin, A., Nadariya, M., Ouzounis, A., Paradissis, D., Peter, Y.,

Prilepin, M., Reilinger, R., Sanli, I., Seeger, H., Tealeb, A., Toksoz, M. N., Veis, G., 2000. Global positioning system constraints on plate kinematics and dynamics in the eastern Mediterranean and Caucasus. Journal of Geophysical Research – Solid Earth 105 (B3), 5695-5719.

McLeod, A., Dawers, N.H., Underhill, J.R., 2000. The propagation and linkage of normal faults: insights from the Strathspey-Brent-Statfjord fault array. Northern North Sea. Basin Research 12, 263-294.

Merritts, D., Vincent, K.R., 1989. Geomorphic response of coastal streams to low, intermediate, and high rates of uplift, Mendocino junction region, northern California. Geological Society of America Bulletin 101 1373-1388.

Milliman, J.D., Syvitski, J.P., 1992. Geomorphic control of sediment discharge to the ocean; the importance of small mountain rivers. Journal of Geology 100, 525-544.

Niemann, J.D., Gasprini, N.M., Tucker, G.E., Bras, R.L., 2001. A quantitative evaluation of Playfair's law and its use in testing long-term stream erosion models. Earth Surface Processes and Landforms 26 (12), 1317-1332.

Över, S., Ünlügenç, U.C., Bellier, O., 2002. Quaternary stress regime change in the Hatay region SE Turkey. Geophysics Journal International 148, 649-662.

Papanikolaou, I., Roberts, G. P., 2006. Geometry, kinematics and deformation rates along the active normal fault system in the southern Apennines: implications for fault growth. Journal of Structural Geology 29, 166-188.

Paton, S., 1992. Active normal faulting, drainage patterns and sedimentation in southwestern Turkey. Journal of the Geological Society (London) 149, 1031-1044.

Pelletier, J. D., 2007. Numerical modeling of the Cenozoic geomorphic evolution of the southern Sierra Nevada, California, Earth and Planetary Science Letters, 259, 85-96.

Pirazzoli, P.A., Laborel, J., Saliège, J.F., Erol, O., Kayan. I., Person, A., 1991. Holocene raised shorelines on the Hatay coasts, Turkey: palaeoecological and tectonic implications. Marine Geology 96, 295-311.

Roberts, G.P., Michetti, A.M., 2004. Spatial and temporal variations in growth rates along active normal fault systems: an example from Lazio-Abruzzo, central Italy. Journal of Structural Geology 26, 339-376.

Saroglu, F., Emre, O., Kuscu, I., 1992. Active fault map of Turkey. Printed by General Directorate of Mineral Research and Exploration, Turkey.

Şengör, A.M.C., Görür, N., & Şaroğlu, F. 1985. Strike-slip faulting and related basin formation in zones of tectonic escape: Turkey as a case study. In: Biddle, K.T, Blick, N.C. (Eds.),

Society of Economic Palaeontology and Mineralogy Special Publication, Tulsa, OK, pp. 37, 227-264.

Snyder, N.P., Whipple, K.X., Tucker, G.E., Merrits, D.J., 2000. Landscape evolution to tectonic forcing: digital elevation model analysis of stream profiles in the Mendocino triple junction region, northern California. Geological Society of America Bulletin 112, 1250-1263.

Steckler, M.S., Berthelot, F., Lyberis, N., Le Pichon, X., 1988. Subsidence in the Gulf of Suez: implications for rifting and plate kinematics. Tectonophysics 153, 249-270.

Tatar, O., Piper, J.D.A., Gürsoy, H., Heimann, A., Koçbulut, F., 2004. Neotectonic deformation in the transition zone between the Dead Sea Transform and the East Anatolian Fault Zone, southern Turkey: a palaeomagnetic study of the Karasu Rift volcanism. Tectonophysics 385, 17-43.

Tucker, G.E., Bras, R.L., 1998. Hillslope processes, drainage density, and landscape morphology. Water Resources Research 34 (10), 2751-2764.

Ministry of Reconstruction and Settlement, 1996. Seismic hazard map of Turkey. Ministry of Reconstruction and Settlement, Ankara, Turkey, 1996.

Van der Beek, P., Bishop, P., 2003. Cenozoic river profile development in the upper Lachan catchment (SE Australia) as a test of quantitative fluvial incision models. Journal of Geophysical Research, 108(B6), doi: 10.1029/2002JB002125.

Wells, D.L., Coppersmith K.J., 1994. New empirical relationships among magnitude, rupture length, rupture width, rupture area and surface displacement. Bulletin of the Seismological Society America, 4 (84), 975-1002.

Westaway, R., Arger, J., 1998. The Gölbaşı basin, southeastern Turkey: a complex discontinuity in a major strike-slip zone. Journal of the Geological Society (London) 153, 729-743.

Whipple, K.X., 2001. Fluvial landscape response time: how plausible is steady-state denundation? American Journal of Science 301, 313-325.

Whipple, K. X., 2004. Bedrock rivers and the geomorphology of active orogens. Annual Review of Earth and Planetary Sciences 32, 151-185.

Whipple, K.X., Tucker, G.E., 1999. Dynamics of the stream power incision model: implications for the height limits of mountain ranges, landscape response timescales and research needs. Journal of Geophysical Research 104, 17,661-17674.

Whipple, K.X., Tucker, G.E., 2002. Implications of sediment-flux dependent river incision models for landscape evolution. Journal of Geophysical Research 107(B2), doi:10.1029/2000JB000044.

Whittaker, A.C., Attal, M., Cowie P.A., Tucker G.E., Roberts, G., 2008. Decoding temporal and spatial patterns of fault uplift using transient river long-profiles. Geomorphology doi:10.1016/j.geomorph.2008.01.018.

Whittaker, A.C., Cowie, P.A., Attal, M., Tucker, G.E., Roberts, G., 2007a. Bedrock channel adjustment to tectonic forcing: implications for predicting river incision rates. Geology 35, 103-106.

Whittaker, A. C., Cowie P. A., Attal, M., Tucker G.E., Roberts, G., 2007b. Contrasting transient and steady-state rivers crossing active normal faults: new field observations from the Central Apennines, Italy. Basin Research 19, 529-556, doi: 10.1111/j.1365-2117.2007.00337.

Wobus, C.W., Whipple, K.X., Kirby E., Snyder, N., Johnson, J., Spyropolou, K., Crosby, B., Sheehan, D., 2006. Tectonics from topography: procedures, promise, pitfalls. In: Willett, S., Hovius, N., Brandon, M., Fisher, D., (Eds.), Tectonics, Climate and Landscape Evolution. AGU Special Paper 398, Geological Society of America, Boulder, CO, pp. 55-74.

Yaltirak, C., Alpar, B., Yuce, H., 1998. Tectonic elements controlling the evolution of the Gulf of Saros (Northeastern Turkey). Tectonophysics 300, 227-248.

Yürür, T., Chorowicz, J., 1998. Recent volcanism, tectonics and plate kinematics near the junction of the African, Arabian and Anatolian plates in the eastern Mediterranean. Journal of Volcanology and Geothermal Research 85, 1-15.

Zelilidis, A., 2000. Drainage evolution in a rifted basin, Corinth graben, Greece. Geomorphology 35, 69-85.